

1 **The influence of multiple groups of biological ice nucleating particles on microphysical**
2 **properties of mixed-phase clouds observed during MC3E**

3
4

5 Sachin Patade^{1*}, Deepak Waman¹, Akash Deshmukh¹, Ashok Kumar Gupta², Arti Jadav¹,
6 Vaughan T. J. Phillips¹, Aaron Bansemer⁴, Jacob Carlin³, Alexander Ryzhkov³,

Moved down [5]: Vaughan T. J. Phillips¹,

Moved (insertion) [5]

7

8 ¹Department of Physical Geography and Ecosystem Science, Lund University, Lund, Sweden

9 ²Department of Earth and Environmental Sciences, Vanderbilt University, Nashville, TN,
10 37240, USA

11 ³Cooperative Institute for Severe and High-Impact Weather Research and Operations, The
12 University of Oklahoma, and NOAA/OAR National Severe Storms Laboratory, Norman,
13 Oklahoma, USA

14 ⁴National Center for Atmospheric Research, Boulder, Colorado, USA

15
16
17
18

19
20
21
22
23

24 *** Corresponding Author**

25 **Dr. Sachin Patade, Lund University, Sweden**

26 **email: sachin.patade@nateko.lu.se**

27
28
29
30

32 **Abstract:**

33 A new empirical parameterization (EP) for multiple groups of primary biological aerosol
34 particles (**PBAPs**) is implemented in the aerosol-cloud model (AC) to investigate their roles
35 as ice-nucleating particles (INPs). The EP describes the heterogeneous ice nucleation by (1)
36 fungal spores, (2) bacteria, (3) pollen, (4) detritus of plants, animals, and viruses, and (5)
37 algae. Each group includes fragments from the originally emitted particles. A high-resolution
38 simulation of a midlatitude mesoscale squall line by AC is validated against airborne and
39 ground observations.

40

41 Sensitivity tests are carried out by varying the initial vertical profiles of the loadings of
42 individual **PBAP** groups. The resulting changes in warm and ice **cloud** microphysical
43 parameters are investigated. **The changes in warm microphysical parameters including liquid**
44 **water content, and cloud droplet number concentration are minimal (< 10%). Overall, PBAPs**
45 have little effect on **ice number concentration (< 6%)** in the convective region. In the
46 stratiform region, increasing the initial **PBAP** loadings by a factor of 1000 resulted in less
47 than **40%** change in ice number concentrations. The total ice concentration is mostly
48 controlled by various mechanisms of secondary ice production (SIP). However, when SIP is
49 **intentionally shut down** in sensitivity tests, increasing the **PBAP** loading by a factor of 100
50 has **less than a 3%** effect on the ice phase. Further sensitivity tests revealed that **PBAPs** have
51 little effect on surface precipitation, as well as on shortwave and longwave flux (**< 4%**) for
52 **100-fold perturbation in PBAPs.**

53

54

55

Deleted: PBAPs

Deleted:

Deleted: PBAP

Deleted:

Deleted: PBAPs

Deleted: the ice phase

Deleted: , especially

Deleted: PBAP

Deleted: 60

Deleted: artificially prohibited

Deleted: PBAP

Deleted: no significant

Deleted: PBAPs

Deleted:

70 **1. Introduction**

71 In most climate models, the largest source of uncertainty for estimating the total
72 anthropogenic forcing is associated with cloud-aerosol interactions (Pörtner et al., 2022).
73 Atmospheric aerosol particles can act as cloud condensation nuclei (CCN) and a few of them
74 act as ice-nucleating particles (INPs), thereby influencing the microphysical properties of
75 clouds and, depending on the cloud type, (Fan et al. 2010; Chen et al 2019). The treatment of
76 INP in climate models can strongly affect the atmospheric radiation budget (DeMott et al.
77 2010). Various sources of aerosol particles, including dust/metallic, marine aerosols,
78 anthropogenic carbonaceous emissions, and primary biological aerosol particles (PBAPs),
79 contribute to the observed INPs (Kanji et al. 2017).

Deleted: ¶

Deleted: Forster

Deleted: 2007

Deleted: -

Deleted: , potentially affecting precipitation formation

Deleted: is control of average cloud particle sizes regulates the radiative properties of layer clouds produced in convection possibly influencing the ...

Deleted: PBAPs

81 A significant amount of global precipitation is associated with the ice phase in cold clouds
82 (Heymsfield and Field 2015; Mülmenstädt et al. 2015, Heymsfield et al. 2020). In particular,
83 mixed-phase clouds are vital for the global climate (Dong and Mace 2003; Zuidema et al.
84 2005; Matus and L'Ecuyer 2017; Korolev et al. 2017 and references therein). In a multimodel
85 simulation study, Tsushima et al. (2006) showed that the doubling of CO₂ concentrations
86 caused the changes in the distribution of cloud-water in the mixed-phase clouds in a climate
87 simulation to be significant.

Deleted: The formation of most

Deleted: S

Deleted:

Deleted: precipitation

Deleted: ly

Deleted: multimodel

Deleted: d

Deleted: Mixed-phase clouds play an important role (about -3.4 Wm^{-2}) in the global net cloud radiative forcing of the present-day climate (e.g., Matus and L'Ecuyer 2017). ...

89 PBAPs are solid particles of biological origin and are emitted from the Earth's surface
90 (Després et al. 2012). They are highly active in initiating ice as INPs and include bacteria,
91 fungal spores, pollen, algae, lichens, archaea, viruses, and biological fragments (e.g., leaf
92 litters, insects) and molecules (e.g., proteins, polysaccharides, lipids) (Després et al., 2012;
93 Fröhlich-Nowoisky et al., 2015; Knopf et al., 2011; Szyrmer and Zawadzki, 1997).

Deleted: PBAPs

Deleted: containing insoluble material

Deleted: Després

Deleted: ö

117 Considering the onset temperature of freezing, some ice nucleation active fungi and bacteria
 118 (especially *Pseudomonas syringae* with onset freezing temperature around -3°C) are among
 119 the most active INPs present in the atmosphere (Després et al. 2012; Hoose and Möhler
 120 2012). The potential impact of PBAP INPs on cloud microphysical characteristics has been
 121 recognized for many years; however, this topic remains a subject of debate (DeMott and
 122 Prenni 2010; Spracklen and Herald, 2014; Hoose et al. 2010b). Some previous modeling
 123 studies have shown that on a global scale PBAPs have only a limited influence on clouds and
 124 precipitation (Hoose et al. 2010; Sesartic et al. 2012, 2013; Spracklen and Heald 2014). On a
 125 global scale, the percentage contribution of PBAPs to the immersion freezing (ice nucleation
 126 by INP immersed in supercooled water drop) is predicted to be much smaller (0.6%) as
 127 compared to dust (87%) and soot (12%) (Hoose et al. 2010).

Formatted: Superscript

Deleted: PBAP

Deleted: . H

Deleted: PBAPs

Deleted: PBAPs

128
 129 Many studies have used cloud models to highlight the potential impact of PBAP INPs on
 130 cloud microphysics and precipitation (e.g., Levin et al. 1987; Grützun et al. 2008; Phillips et
 131 al. 2009). For example, the mesoscale aerosol-cloud model by Phillips et al. (2009) had a 3-D
 132 domain of about 100 km in width, and many cloud types were present in the mesoscale
 133 convective system that was simulated. Their simulations revealed that the cloud cover,
 134 domain radiative fluxes, and surface precipitation rate were significantly altered by boosting
 135 organic aerosols representing PBAPs. According to Hummel et al. (2018) in shallow mixed-
 136 phase clouds (i.e., altostratus) when the cloud top temperature is below -15°C, PBAPs have
 137 the potential to influence the cloud ice phase and produce ice crystals in the absence of other
 138 INPs.

Deleted: PBAP

Deleted: ;

Deleted: Hummel et al. 2018

Deleted: PBAPs

Deleted: PBAPs

149 The quest for insights into the broader atmospheric role of PBAP INPs for cloud
 150 microphysical properties and precipitation is hampered by the limited availability of
 151 observations both of their ice nucleation activities for various species and their aerosol
 152 distributions in the real atmosphere (Huang et al. 2021). More generally, there is incomplete
 153 knowledge about the chemical identity of the key INPs, whether biological or otherwise
 154 (Murray et al. 2012). In many global and regional models, the ice nucleation activity of
 155 bioaerosols is represented either empirically or theoretically based on laboratory
 156 measurements of specific biological species of PBAPs that are assumed as representative
 157 candidates (e.g., *Pseudomonas syringae*). This assumption of representativeness introduces
 158 uncertainties that would be expected to impact the model results, potentially introducing a
 159 bias into the estimation of the effects of bioaerosols on clouds (e.g. Sahyoun et al., 2016;
 160 Hoose et al. 2010b; Spracklen and Herald, 2014, Huang et al. 2021 and references therein).

Deleted: about

Deleted: PBAP

Deleted: PBAPs

162 In addition to primary ice nucleation, ice formation in clouds can occur because of processes
 163 generating new particles from pre-existing ice, and these are known as Secondary Ice
 164 Production (SIP) mechanisms (Korolev and Leisner, 2020; Korolev et al. 2020). SIP can have
 165 a considerable impact on cloud micro- and macro-physical properties such as precipitation
 166 rate, glaciation time, cloud lifetime, and cloud electrification by increasing the ice number
 167 concentrations by a few orders of magnitude (e.g., Blyth and Latham 1993; Crawford et al.,
 168 2012; Lawson et al., 2015; Phillips et al., 2017b, 2018, 2020; Phillips and Patade, 2021;
 169 Sotiropoulou et al. 2021a,b). This in turn can influence the global hydrological cycle and
 170 climate. For example, Zhao and Liu (2021) demonstrated using a global climate model that
 171 SIP dominates ice formation in moderately cold clouds and has a significant influence on
 172 their liquid and ice water paths. They showed that including three SIP mechanisms in the
 173 model simulated global annual average liquid water path decreases by 15 g m⁻² (-22%

Deleted: modifying

Deleted: the

Deleted: of ice particle concentrations

Deleted: (

Deleted:)

Deleted: -

183 change) and the ice water path increases by 9 g m^{-2} (23%), resulting in better agreement with
184 observations. Accounting for SIP in their model results in a change in the global annual
185 average net cloud radiative forcing by about 1 W m^{-2} . Although a small fraction of the total
186 cloud radiative forcing globally, this flux change underlines the ubiquitous role of SIP on
187 cloud properties on the large scale.

Deleted: this is

188

189 However, in many cloud models, the representations of these SIP mechanisms are uncertain
190 as most of the cloud models include only the Hallet-Mossop (hereafter HM; Hallett and
191 Mossop, 1974) process and neglect other SIP mechanisms (e.g. Fan et 2017; Han et al 2019).
192 A few secondary ice formation processes (e.g., the HM process) have been suggested to be
193 active in the temperature range where active PBAP INPs exhibit strong ice nucleation
194 activity. The INPs of biological origin such as bacteria are highly active in the temperature
195 range of the HM process (-3 to -8°C) as compared with non-biological INPs (Möhler et al.
196 2008; Patade et al., 2021, henceforth PT21). At temperatures warmer than -15°C, some of the
197 PBAPs generated by biologically active landscapes (e.g. forests, woodlands) can promote ice
198 formation and crystal growth in clouds (Morris et al., 2014).

Deleted: s

Deleted: Hallet-Mossop, 1974

Deleted: PBAP

Deleted: the Hallet-Mossop (

Deleted:)

Deleted: PBAPs

199

200 In the USA, about 18% of the total landmass is used as cropland, farmland, and agricultural
201 activities (Garcia et al. 2012). These are major sources of biological particles in the
202 atmosphere. Biogenic particles released from crops, either pre- and post-harvest, have
203 previously been shown to serve as INPs (in Colorado and Nebraska, Garcia et al. 2012).
204 Huffman et al. (2013) found that airborne biological particles increase significantly in
205 concentration, by an order of magnitude or more, during rainfall in a forest in the western US
206 and that bioaerosols are well correlated with INPs. Prenni et al. (2013) observed a similar

Deleted: (

215 increase in concentrations of ground-level INPs during rain at a forested site in Colorado,
216 which was associated with increased biological particles. If these potential INPs are detrained
217 from the convective outflow of a cell at mid-levels, then they may be entrained into other
218 clouds aloft, influencing the microphysical properties of that subsequent storm. Convective
219 clouds can efficiently transport lower tropospheric aerosol particles into the upper
220 troposphere where they can affect the cloud properties (Cui and Carslaw, 2006)

221

222 The current study aims to simulate realistic concentrations of multiple groups of PBAP INPs,
223 including bacterial and fungal particles, to investigate their interactions with convective
224 clouds observed during the Midlatitude Continental Convective Clouds Experiment field
225 campaign (MC3E), in the USA (Jensen et al. 2016), in the USA. In view of the literature
226 noted above about the effects of PBAP INPs, there is a need for more detailed analyses of
227 their role in altering cloud microphysical properties and precipitation because the realistic
228 treatment of ice nucleation activity for major PBAP groups was not available, prior to our
229 empirical scheme (PT21). Hitherto, laboratory measurements of isolated biological species
230 (e.g., *Pseudomonas syringae*, *Cladosporium sp*) have been the basis for attempts to simulate
231 biological ice nucleation in clouds, but the representativeness of the choice of such species
232 has been a longstanding issue. For example, Hummel et al (2018) considered three highly ice-
233 nucleation-active PBAP species in their model which may not represent the ice nucleation
234 activity of PBAP in the atmosphere. It is not known which biological species of ice
235 nucleation active (INA) PBAPs contribute the most to biological ice nucleation.
236 Consequently, there is a need for a new approach oriented toward laboratory measurements
237 of biological INPs sampled from the atmosphere, thus optimizing the representativeness of
238 the data for studies of clouds.

Deleted: PBAP

Deleted: from

Deleted: PBAP

Deleted: IN

Deleted: PBAP

Deleted: Patade et al. 2021

Deleted: INA

Deleted: PBAPs

Deleted: natural

Deleted: real

Deleted: natural

250

251 In this paper, such an approach is followed to investigate the effect on cloud properties from
252 various major groups of PBAP. We incorporated a recent empirical parameterization for
253 various PBAP groups by PT21 into our 3D aerosol-cloud model (AC). PT21 created an
254 empirical formulation resolving the ice nucleation of each group of PBAPs including 1)
255 fungal spores and their fragments, 2) bacteria and their fragments, 3) pollen and their
256 fragments, 4) detritus of plants, animals, and viruses, and 5) algae. The empirical formulation
257 by PT21 is based on observations of PBAP collected at the Amazon Tall Tower Observatory
258 (ATTO). It is a research site located in the middle of the Amazon rainforest in northern
259 Brazil. In this article, we also examine the relative importance of various secondary ice
260 processes in their role in mediating the PBAP effects on cloud microphysical properties,
261 given the weakness of PBAP effects on cloud microphysical properties.

262

263

264 **2. Description of observations**

265 *2.1 Selected case of a deep convective system*

266 In the current study, we simulated a squall line that occurred on 20 May 2011 MC3E
267 (Jensen et al. 2016). The MC3E campaign took place from 22 April through to 6 June 2011
268 and was centered at the Atmospheric Radiation Measurement (ARM) Southern Great Plains
269 (SGP) Central Facility (CF), (36.6°N, 97.5°W) in north-central Oklahoma. Jensen et al.
270 (2016) describe the squall line as a "golden event" of the MC3E campaign given the robust *in*
271 *situ* sampling of extensive stratiform outflow from deep convection on this day. The surface
272 meteorological analysis on 20 May indicated a southerly flow at the surface, which provided
273 enough moisture from the Gulf of Mexico to trigger convection. Deep convection, organized

Deleted: PBAP

Deleted: PBAP

Deleted: Patade et al. (2021, henceforth PT21)

Deleted: PBAPs

Deleted: ¶

¶
The paper is structured as follows. In the next two sections, the methodology for the model setup and a description of the observed storm simulated. The subsequent section shows results comparing simulated cloud properties with observations to validate the model. There follows the analysis of sensitivity tests concerning the loading of PBAPs.

Deleted: PBAP

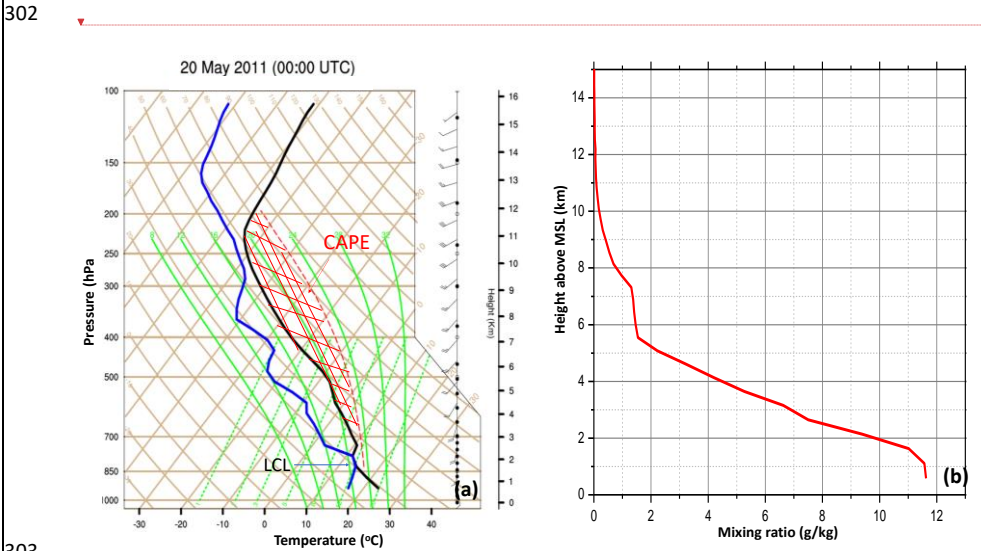
Deleted: PBAP

Deleted: of field campaign

Deleted: in view of

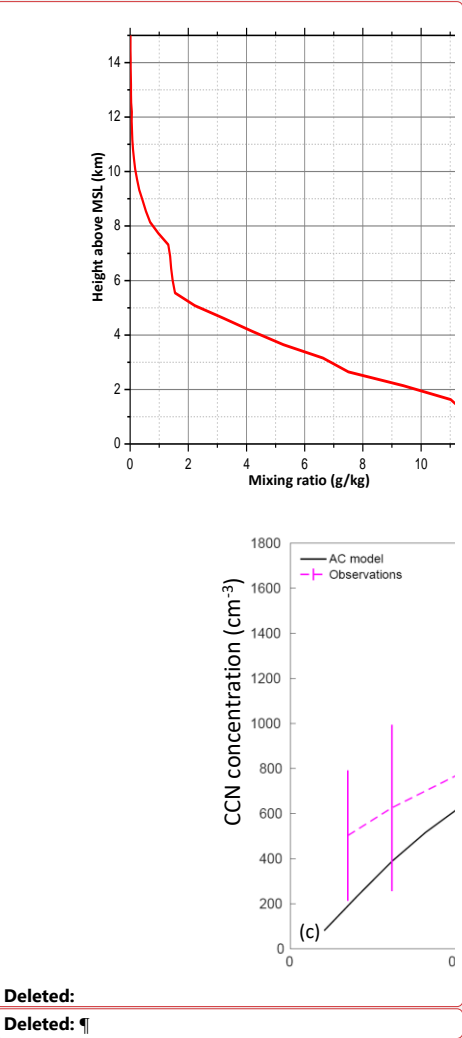
290 in the form of a squall line, passed over the measurement site between 1030 and 1100 UTC,
291 resulting in convective precipitation. It was followed by widespread stratiform precipitation
292 that was well observed by both airborne and ground-based measurements.

293
294 The skew- T plot from the radiosonde sounding conducted on 20 May 2011, at (00 UTC) is
295 shown in Figure 1a. The skew- T plot shows the vertical sounding before the formation of
296 deep convection. The skew- T plot shows that the surface-based Convective Available
297 Potential Energy (CAPE) for this case was 2400 J kg^{-1} , and the Lifting Condensation Level
298 (LCL) was located at 840 hPa. The temperature at LCL, which is generally at the same height
299 as the convective cloud base, was 15°C . The vertical profile of the water vapor mixing ratio is
300 also shown in Figure 1b. The water vapor mixing ratio at the surface was around 11.8 g kg^{-1}
301 which decrease rapidly to 2 g kg^{-1} at 5 km.



303 **Figure 1.** (a) The skew T plot from May 20, 2011, sounding. The air temperature is
304 represented by the solid black line, while the dew point temperature is represented by a
305

Deleted: supplementary
Deleted: 2355
Deleted: 9
Deleted: 4
Deleted: supplementary
Deleted: figure S1b
Formatted: Superscript
Deleted: The estimated amount of vapour in the entire depth of the troposphere corresponded to precipitable water of 3 cm. ¶



317 dashed grey line. The moist adiabat is represented by a dotted red line. The shaded region
 318 between moist adiabat and temperature line represents convective available potential energy
 319 (CAPE). The LCL is also mentioned in the plot. (b) Vertical profile of water vapor mixing
 320 ratio on 20 May 2011 at 00 UTC.

323 2.2 Aircraft Observations

324 The *in situ* cloud microphysical observations used in this study were obtained from a
 325 University of North Dakota Citation II aircraft. The aircraft collected observations of cloud
 326 microphysical parameters from the cloud base (1.8 km above MSL) to a maximum altitude of
 327 7.5 kilometers above MSL. The MC3E campaign collected extensive airborne measurements
 328 of aerosols and cloud microphysical properties over north-central Oklahoma. A detailed
 329 description of the scientific objectives of the MC3E program, including the field experiment
 330 strategy, airborne and ground-based instrumentation, is given in the paper by Jensen et al.
 331 (2016). This section summarizes the instrumentation used in the current study.

332 **Table 1:** Details of aircraft instruments used in this study.

Instrument	Measurement	Typical range
Cloud imaging probe (CIP) by Droplet Measurement Technologies (DMT)	Size distribution of cloud and precipitation particles	0.025–1.5 mm (0.2–1 mm for model validation in the current study)
2D cloud imaging probe (2D-C) (PMS)	Size distribution of cloud and precipitation particles	0.03–1.0 mm (0.2–1 mm for model validation in the current study)
Cloud droplet probe (CDP) (DMT)	Cloud droplet spectra	2–50 μm
High-volume precipitation	Precipitation particle	0.15–19.2 mm

Deleted: Figure 1. (a) Vertical profile of water vapor mixing ratio on 20 May 2011 at 00 UTC. (b) The skew T plot from May 20, 2011, sounding. The air temperature is represented by the solid black line, while the dew point temperature is represented by a dashed grey line. The moist adiabat is represented by a dotted red line. (c) The CCN spectrum from AC for a simulated squall line case on May 20, 2011, for an environment 500 meters above MSL. The predicted CCN spectrum is compared to the observed CCN spectrum at the SGP CF (300 m above MSL)....

Formatted: Line spacing: Double

Deleted: ¶

Deleted: kilometres

spectrometer, version 3 (HVPS-3) (SPECinc)	spectra	
King hot-wire liquid water content (LWC) probe (DMT)	Cloud liquid water	0.01–5 g m ⁻³
Temperature probe	Ambient air temperature	—
Static pressure sensor	Ambient air pressure	—

The Citation aircraft was equipped with a standard suite of meteorological instruments, which provided high-resolution measurements of temperature, pressure, and humidity. In addition, it carried microphysical probes for cloud and precipitation, and liquid water content, as listed in Table 1.

Particle size distributions (PSDs) from cloud to precipitation particle sizes were measured with various probes, including a 2D Cloud Imaging Probe (2D-C), a Cloud Imaging Probe (CIP), and a High-Volume Precipitation Spectrometer Probe (HVPS). The 2D-C and CIP probe data were processed objectively using the algorithm developed at the National Center for Atmospheric Research (NCAR) to mitigate artifacts produced by shattering on the probes' leading edges (Field et al. 2006). The 2D-C probe was equipped with anti-shattering tips (Korolev et al., 2011), while the CIP did not have anti-shattering tips. The size distribution of cloud drops with diameters from 2 to 50 μm was measured using a Cloud Droplet Probe (CDP). A King hot-wire liquid water content (LWC) probe measured the LWC. Vertical velocity is derived from air motion sensing systems available on the research aircraft.

Deleted: Korolev

2.3 Ground-based measurements

365 A comprehensive instrumentation suite deployed at the ARM-SGP central facility provided
366 continuous measurements of atmospheric gases, aerosols, clouds, and local meteorological
367 conditions (e.g., wind, temperature, precipitation, and atmospheric profiles). A cloud
368 condensation nuclei (CCN) counter (CCN-100) (DMT) measured the CCN number
369 concentration at seven supersaturation values with a temporal resolution of 1 hour. Surface
370 precipitation was measured with 16 rain gauge pairs placed within a 6-kilometer radius of the
371 SGP CF.

372
373 During the MC3E campaign, the measurement facility deployed at CF measured the spatial
374 variability of surface fluxes of heat, moisture, and momentum. A radiosonde array of 6 sites,
375 covering an area of 300 km × 300 km, was designed to capture the large-scale variability of
376 the atmospheric state. Radiosonde observations (Vaisala RS92-SGP) were conducted with a
377 6-hour frequency (four times daily) at around 05:30, 11:30, 16:30, and 22:30 UTC, providing
378 vertical profiles of atmospheric state variables (pressure, temperature, humidity, and winds)
379 of the environment surrounding the ARM SGP site. When aircraft operations were planned
380 based on forecasted convective conditions, the sounding frequency was increased to a 3-hour
381 frequency with the starting time at 05:30 UTC.

382
383 In addition to airborne observations, the ARM radar network was used to conduct unique
384 radar observations during the MC3E campaign. The information about various radar assets
385 during MC3E is given by Jensen et al. (2016). The surface precipitation used for model
386 validation in this study is a radar-based precipitation estimate as described by Giangrande et
387 al. (2014). They used radar observations from the C-band and X-band scanning ARM
388 precipitation radars (C-band Scanning ARM Precipitation Radar and X-band Scanning ARM

Deleted: extended

Deleted: to eight times per day.

Deleted: ¶

Deleted: heterogeneous

Deleted: Giangrande

Precipitation Radars, respectively) to estimate rainfall within 100 km of the ARM facility in Lamont, Oklahoma. Their radar-based rainfall retrievals were in good agreement with observations with an absolute bias of less than 0.5 mm for accumulations less than 20 mm.

Deleted: to

The Interagency Monitoring of Protected Visual Environments (IMPROVE) network stations close to the location of airborne observations provided ground-level measurements of various chemical species. These included carbonaceous compounds (black and organic carbon), salt, ammonium sulfate, and dust. The details of the measurement techniques used for mass mixing ratios of these compounds are summarized in Malm et al. (1994). The measurements of these aerosol species from various IMPROVE sites, including Ellis (36.08°N, 99.93°W), Stilwell (35.75°N, 94.66°W), and Wichita Mountains (34.73°N, 98.71°W) sites in Oklahoma, were averaged to provide inputs to AC. Initial mass concentrations for the aerosol species of AC (11 species) including sulfate, sea salt, dust, black carbon, soluble organic, biological and non-biological insoluble organic (five groups of PBAPs) were derived from the Goddard Chemistry Aerosol Radiation and Transport (GOCART) model (Chin et al. 2000). The prescribed mass mixing ratios of aerosol species in A are based on IMPROVE observations and are enlisted in Table 2. It should be noted that for the MC3E case considered in this study, coincident IMPROVE measurements were not available. The mean values of the IMPROVE measurements conducted on May 18 and 21 are used to prescribe the mass of various aerosol species.

Deleted: 10

Deleted: and insoluble organic (five groups of bioaerosols) were derived from ...

Moved (insertion) [1]

Deleted: Profiles of aerosol mass concentration were scaled at all levels to match simultaneous measurements by IMPROVE. ...

Deleted: C-

Moved up [1]: The prescribed mass mixing ratios of aerosol species in AC-based IMPROVE observations are enlisted in Table 2.

Deleted: The prescribed mass mixing ratios of aerosol aerosol species in AC-based IMPROVE observations are enlisted in Table 2....

Table 2: The mass mixing ratio of aerosol species based IMPROVE observations which are used as input to AC.

Aerosol species	Mass mixing ratio ($\mu\text{g}/\text{m}^3$)
(NH ₄) ₂ SO ₄	0.56
Dust	0.18
Sea salt	0.021

Black carbon	0.093
Soluble organic carbon (80 % of TOC)	0.45
Insoluble organic carbon (20 % of TOC)	0.18
PBAPs (50% of Insoluble organic carbon)	FNG=0.036; BCT=0.012; PLN=0.028; DTS=0.016; ALG=0.000022

Deleted: PBAPs

3. Methodology

3.1 Model description

The ‘aerosol-cloud model’ (AC) used in this study is a cloud-resolving model (CRM) with a hybrid spectral bin/two-moment bulk microphysics, interactive radiation, and semi-prognostic aerosol schemes (Phillips et al. 2017a, 2020). The model predicts the mass and number concentrations for five types of hydrometeors: cloud liquid, cloud ice (or “crystals”), rain, graupel/hail, and snow. The mixing ratios of the total number and mass of all particles in each microphysical species are treated as model prognostic variables. AC treats all known microphysical processes such as droplet nucleation, ice initiation through primary and secondary processes, and growth processes such as deposition/sublimation of ice particles, condensation/evaporation of drops, freezing/melting, as well as coagulation by collisions between various hydrometeor types. Both cloud-base and in-cloud activation of aerosols to form cloud-droplets are treated explicitly, with the predicted in-cloud supersaturation resolved on the model grid being used to activate aerosols aloft. Bin-resolved size distributions of each aerosol species are predicted for the interstitial and immersed

449 components of each aerosol species. Extra prognostic variables track the number of aerosols
450 in each aerosol species that have been lost by INP and CCN activation.

451

452 Secondary ice formation is represented by four types of fragmentation:

- 453 • breakup in ice–ice collisions (Phillips et al. 2017a, b) (most active between -10 to -
454 20°C);
- 455 • Hallett and Mossop (1974), rime splintering (most active between -3 to -8°C) ;
- 456 • fragmentation of freezing rain/drizzle by modes 1 and 2 (Phillips et al. 2018) (most
457 active around -15°C);
- 458 • and sublimation breakup (Deshmukh et al. 2021) (most active between -0 to -18°C).

Deleted: ,

Deleted: ,

Formatted: Superscript

Formatted: Superscript

459 The empirical parameterization (EP) (Phillips et al. 2013) of heterogeneous ice nucleation
460 treats all known modes of ice formation (deposition mode, condensation-/immersion-
461 freezing, inside-out and outside-in contact-freezing) in terms of dependencies on the loading,
462 size, and chemistry of multiple aerosol species. In the previous version of the EP, prior to
463 PT21, there were four species of INP aerosol. One of these was PBAP INPs. However, that
464 version of the EP did not resolve the individual types of PBAP INP, which exhibit a wide
465 range of ice-nucleating abilities. The current version of AC also includes the ice nucleation
466 (IN) activity of dust and black carbon. The ice nucleation parameterization of dust, as well as
467 black carbon, is based on studies by Phillips et al. (2008) and (2013). The activation of dust
468 and black carbon INP starts at temperatures colder than -10 and -15°C.

Deleted: PBAP

Deleted: PBAP

Deleted: as well as black carbon

Formatted: Superscript

469

470 There are two types of homogeneous freezing represented: that of cloud droplets near -36°C
471 and that of solute aerosols at colder temperatures. Both schemes are described by Phillips et

477 al. (2007, 2009). For cloud droplets, a look-up table from simulations with a spectral bin
478 microphysics parcel model treats the fraction of all supercooled cloud droplets that evaporate
479 without freezing near -36°C, depending on the ascent, initial droplet concentration and
480 supersaturation. The size dependence of the temperature of homogeneous freezing is
481 represented.

482
483 In a recent study, PT21 provided an empirical formulation for multiple groups of **PBAP** INPs
484 based on field observations over the central Amazon. In this study, we modified AC by
485 implementing the recent empirical parameterization of **PBAP** INPs by PT21. A summary of
486 their formulation is provided in section 3.2.

Deleted: ¶

Deleted: A

Deleted: PBAP

Deleted: PBAP

487
488 Cloud processes and rainfall formation have been detected using different radar variables,
489 such as specific differential phase K_{DP} . Moisseev et al. (2015), for example, noted an increase
490 in observed K_{DP} because of aggregation. In addition, a few studies have hypothesized
491 evidence of SIP via K_{DP} (e.g., Sinclair et al. 2016; Kumjian and Lombardo 2017; Carlin et al.
492 2021). In this study, we attempted to detect secondary ice formation signatures by
493 implementing K_{DP} estimations into AC. Based on Ryzhkov et al. (2011), K_{DP} values were
494 estimated for various hydrometeor types, including cloud drops, raindrops, cloud ice, snow,
495 and graupel (their equations 22, 23, 24, 26, and 29). The scattering amplitudes were
496 calculated using the Rayleigh approximation. The K_{DP} estimations are made for 0° elevation
497 angle and S-band (radar wavelength of 11 cm). The equivalent volume diameter of the given
498 hydrometeor was used for all calculations.

499
500 *3.2 Empirical formulation for **PBAP** INPs:*

Deleted: PBAP

506 The empirical formulation by PT21 for multiple groups of PBAPs includes: - 1) fungal spores
 507 (FNG), 2) bacteria (BCT), 3) pollen (PLN), 4) viral particles, plant/animal detritus (DTS), 5)
 508 algae (ALG) and their respective fragments are implemented in AC. This formulation is
 509 based primarily on field observations over the central Amazon rainforest, with empirically
 510 derived dependencies on the surface area of each group (except algae) and it applies to the
 511 particles with diameters greater than 0.1 μm . Here, we summarize the formulation by PT21
 512 briefly.

513 For $X = \text{FNG, PLN, BCT, and DTS}$

$$514 \quad n_{IN_BIO,X} = \int_{\log [0.1 \mu\text{m}]}^{\infty} \{1 - \exp [-\mu_X]\} \times \frac{dn_X}{d\log D_X} d\log D_X, \quad (1)$$

$$515 \quad \mu_X = H_X(S_i, T) \xi(T) \times \text{MIN}\{\exp(-\gamma_X T) - 1, 40\} \times \frac{1}{\omega_{X,1*}} \frac{d\Omega_X}{dn_X} \text{ for } T < 0^\circ\text{C} \quad (2)$$

516 In equation (1), $n_{IN_BIO,X}$ is the number mixing ratio of INP active at temperature T for given
 517 species X ; Ω_X is the total surface area mixing ratio of particles with diameters D_X greater than
 518 0.1 μm ; $d\Omega_X/dn_X \approx \pi D_X^2$. The normalized size distribution of given bioaerosol species is
 519 given by $dn_X/d\log D_X$. In Eq (2), H_X is the empirically determined fraction that inhibits
 520 nucleation in substantially water-subsaturated conditions. The factor ξ varies between 0 to 1
 521 and considers the fact during laboratory experiments drop freezing was not observed at
 522 temperatures warmer than a certain threshold in the laboratory observations. The parameter
 523 $\omega_{X,1*}$ depends on bioaerosol type with the dimensions of area (m^2). The values of
 524 $\omega_{X,1*}$ shown for PLN and DTS are 0.1 m^2 . For FNG and BCT the values of $\omega_{X,1*}$ are
 525 9.817×10^{-5} and 9.12×10^{-5} m^2 respectively. The slope of the fitted curve (γ_X) has a
 526 constant value of 0.5 C^{-1} .

Deleted: PBAPs

Deleted: including:-

Formatted: Font: Italic

Deleted: which

Deleted: em

532 The concentration of algal particles at the ATTO site was much smaller than our detection
 533 threshold, so we could not use a similar empirical treatment for ALG. The frozen fraction for
 534 the algal particles (Diatom cell, *Thalassiosira pseudonana*) available in the literature is used
 535 to estimate INPs from ALG (Wilson et al. 2015). The frozen fraction is given by eq. (3)

$$f_{algae}(T) = A_1 + \frac{(A_2 - A_1)}{1 + 10^{(B+T) \times p}} \quad (3)$$

537 where $A_1 = -0.03$, $A_2 = 0.993$, $B = 27.73$, and $p = 0.399$.

538 Also $f_{algae}(T) = 0$ at $T > -24^\circ\text{C}$ and $f_{algae}(T) = 1$ at $T < -35^\circ\text{C}$

539 For the given concentration of algal particles in the air (n_{algae}) the active INP from ALG is
 540 given by

$$n_{IN,BIO,X} = f_{algae} \times n_{algae} \quad (4)$$

544 3.3 Model setup

545 AC was driven by initial and evolving boundary data for meteorological conditions. The
 546 large-scale advection of humidity and temperature tendencies maintained the convection.
 547 Convection was initiated by imposing perturbations onto the initial field of vapour mixing
 548 ratio. The large-scale forcing condition used for the simulation was derived using the
 549 constrained variational analysis method described in Xie et al (2014). Based on this method,
 550 the so-called large-scale forcing including large-scale vertical velocity and advective
 551 tendencies of temperature and moisture were derived from the sounding measurements
 552 network. During the MC3E campaign, the sounding network consists of five sounding
 553 stations centered on a sixth site at the ARM SGP central facility (CF). An area with a

Deleted: s

Deleted: Amazon Tall Tower Observatory (

Deleted:)

Deleted: were

Deleted: , T. pseudomonas

Deleted: PT21 elaborate further.

Deleted: are

Formatted: Indent: First line: 0 cm

Moved (insertion) [2]

Deleted: (

Deleted: .

Deleted: ;

Deleted: Jensen et al. 2016

Deleted:)

diameter of approximately 300 km was covered by this sounding network covers. Additional details about the sounding data are described in section 2.3. Figure S1 shows the time height evolution of potential temperature and water vapor mixing ratio from large-scale forcing data. It also shows the time variation of CAPE based on observations. The maximum value of CAPE 2400 JKg⁻¹ was noticed around 12 UTC on 20th May.

Deleted: provides additional details about

Deleted: for the simulated time period

Deleted: ¶

Formatted: Superscript

Formatted: Superscript

Formatted: Tab stops: 12,28 cm, Left

The model simulations were carried out for a three-dimension domain of 80 km x 80 km with horizontal grid spacings of 2 km. In vertical, the model resolution was 0.5 km, and the model top was located at about 16 km. The lateral boundary conditions are doubly periodic on all sides of the domain. The initial time of the simulations was at 1200 UTC on 19 May 2011 and all simulations were performed for 48 hours at a time step of 10 seconds.

Deleted: domain

Moved up [2]: The large-scale forcing condition used for the simulation was derived using the constrained variational analysis (Xie et al. 2014; Jensen et al. 2016). The initial time

The GOCART model (Chin et al. 2000) was used to initialize the seven chemical species associated with the EP. The data from the three IMPROVE sites mentioned above (Section 2.3) was used to rescale the mass concentration profiles at all levels so that they match the measurements near the surface. Table 2 lists the mass mixing ratios of various aerosol species after the corrections. The corresponding vertical profiles of various aerosol species including sulfate, dust, sea salt, black carbon, and total organic carbon are shown in Supplementary Figure S2 (panel a-e). The corresponding IMPROVE measurements are also shown in the same Figure. There were no direct measurements of PBAP mass during IMPROVE and therefore it was derived from the measured mass of the total organic carbon (TOC). The relative contribution of insoluble and soluble organic carbon to TOC was assumed to be 20% and 80%, respectively by assuming a water-soluble fraction of 80% for carbonaceous aerosol (Phillips et al. 2017b). AC takes into account the soluble fraction of each type of aerosol. The

Deleted: 1

Deleted: the total organic carbon (

Deleted:)

600 values of this factor are 0.15 for dust, and 0.8 for carbonaceous species. The value of this
601 fraction for all PBAP groups is 0.1.

602
603 There are very observations available in the literature showing the fraction of PBAP in the
604 insoluble organics or total aerosol particles. For example, observations by Matthias-Maser et
605 al. (2000) found that 25% of the total insoluble particles are biological. PBAPs can contribute
606 a significant fraction to the number concentrations of total aerosol particles (Mattias-Maser et
607 al., 1999). Mattias-Maser and Jaenicke (1995) showed that PBAPs can amount to 20% and
608 30% of the total aerosol particles. The observation by Jaenicke (2005) in a semi-rural location
609 showed that cellular particles can contribute up to about 50% of total particles. Based on
610 these studies we assumed that 50% of the insoluble organics were biological in origin. The
611 total PBAP loading was prescribed partly based on observations of insoluble organics. The
612 mass fraction of each PBAP group in total PBAP mass is prescribed based on the PT21
613 observations. The fraction of mass mixing ratio for various PBAP groups is: FNG= 0.39,
614 BCT= 0.13; PLN= 0.31; DTS= 0.17; ALG= 2.5×10^{-4} .

615
616 It should be noted that the observations of PBAPs over different geographical locations
617 (including the region where we carried out the simulation) are rare, which prevents us from
618 using the region-specific PBAP observations for the present study. Hence, PT21's default
619 observations were used to calculate the relative contribution of various PBAP groups to
620 insoluble organics. The parameters for the shape of PSD of each PBAP group (modal mean
621 diameters, standard deviation ratios, and relative numbers in various modes) are prescribed
622 based on observations from Amazon (PT21). Supplementary Figure S3 depicts the
623 corresponding size distribution of various PBAP groups in AC. The figure depicts unimodal

Deleted: Due to a lack of observational data, it was

Deleted: parsimoniously

Deleted: PBAP

Deleted: and partly

Deleted: assumed fraction.

Deleted: PT21's observations were used to calculate the relative contribution of various PBAPPBAP groups to insoluble organics. ...

size distribution for FNG, BCT, PLN, and ALG, whereas DTS has a bimodal size distribution. To check the validity of the observation from PT21 over the region considered in the current study, the model estimated values of one of the major PBAP bacteria are compared with the observations as shown in Figure S4. It shows that the estimated values of bacterial number concentration are overall in fair agreement with previous observations (e.g. Bowers et al 2009; Bauer et al. 2002; Burrows et al. 2009). The simulated bacterial ($\sim 10^4 \text{ m}^{-3}$) and fungal ($\sim 10^3 \text{ m}^{-3}$) number concentration by AC is in good agreement with their typical concentration in the atmosphere (Després et al. 2012). The resulted vertical profiles of mass of the various PBAP groups are shown in Figure S2 (panel f).

Deleted: l

From these prescribed loadings of aerosol species, AC predicts their size distribution and hence the CCN activity spectrum. Using the initial sounding and aerosol profile, AC can predict the in-cloud size distribution of aerosols in each species as well as in-cloud supersaturation. To validate this prediction, Figure 2 shows the predicted CCN spectrum compared with observations from the CCN counter at the surface at the SGP site.

Deleted: The parameters for the shape of PSD of each PBAPPBAP group (modal mean diameters, standard deviation ratios, and relative numbers in various modes) are prescribed based on observations from Amazon (PT21). ¶

Deleted: l

Deleted: c

It should be noted that the aerosol mass loading from IMPROVE observations showed variations of 20-30% for the simulated case. The uncertainties in the input aerosol mass loading can result in simulated CCN concentration and are shown by the errors in the CCN concentration predicted by the AC. During 19-20 May, the measured number concentration of active CCN at the SGP CF ranged from 400 to 3000 cm^{-3} at 1% supersaturation (Fridlind et al. 2017). The measurements were made on 20 May before the start of the rain in clear air.

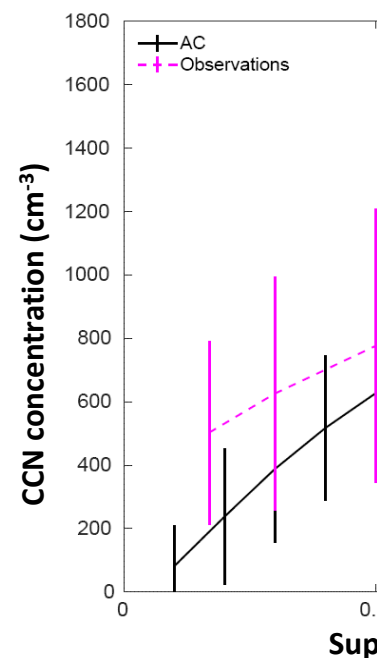
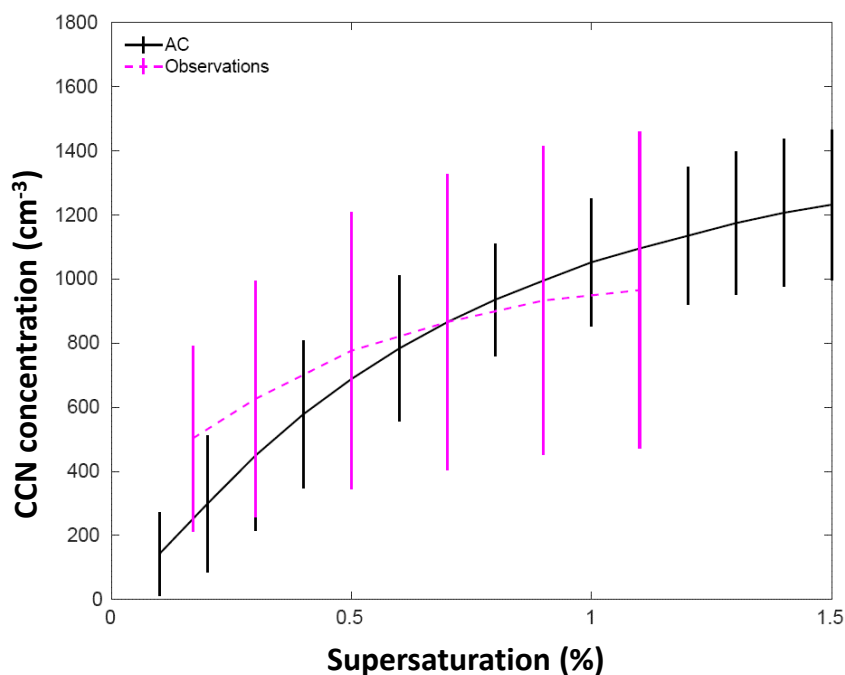


Figure 2. The CCN spectrum from AC for a simulated squall line case on May 20, 2011, for an environment 500 meters above MSL. The predicted CCN spectrum is compared to the observed CCN spectrum at the SGP CF (300 m above MSL). The error bars on the model predicted CCN concentration are associated with uncertainties in the input values of mass mixing ratios of various aerosol species that act as CCN.

The normalized CCN number concentrations at 1% supersaturation from observations and AC are $\sim 1000 \text{ cm}^{-3}$ and $\sim 940 \text{ cm}^{-3}$, respectively. Given the wide range of observed CCN concentrations at each supersaturation as well as the uncertainties in the model predicted CCN concentration, the predicted and observed CCN activity spectra are in acceptable agreement.

Deleted: 1

Deleted: It should be noted that the aerosol mass loading from IMPROVE observations showed variations of 20-30% for the simulated case. The uncertainties in the input aerosol mass loading can result in simulated CCN concentration and are shown by the errors on the CCN concentration predicted by the AC. During 19-20 May, the measured number concentration of active CCN at the SGP CF ranged from 400 to 3000 cm^{-3} at 1% supersaturation (Fridlind et al. 2017). The measurements were made on 20 May before the start of the rain in clear air. ...

Deleted: good

689

690 4. Results from control simulation and model validation

691 4.1 Overview of the control simulation

692 An intense north-to-south oriented squall line moved over the ARM SGP CF on May 20,
693 2011, from 1100 to 1400 UTC (Sec. 2.1). The new version of AC simulated this case, after
694 implementing the empirical formulation by PT21 for multiple groups of PBAP INPs
695 ('control' simulation) (Sec. 3). It should be noted that five ensemble runs were carried out for
696 control simulation (See Table 3) varying the perturbing in the initial water vapor mixing
697 ratio.

698

699 Figure 3 shows the time-height evolution of various liquid and ice cloud microphysical
700 parameters derived from the control simulation conditionally averaged over cloudy regions.
701 The maximum average cloud droplet number concentration was around 250 cm^{-3} . The LWC
702 was typically less than 0.5 g m^{-3} . The freezing level (0°C) was around 4.1 km above MSL.
703 The deep convection began around 10 UTC, followed by intense precipitation around 11
704 UTC, and reached its peak around 12 UTC. The time-height evolution of cloud ice, snow,
705 and graupel number concentrations shows maxima shortly before 12 UTC, which coincides
706 with the time of peak precipitation. This suggests that the ice phase was important in
707 precipitation formation.

708

Deleted: PBAP

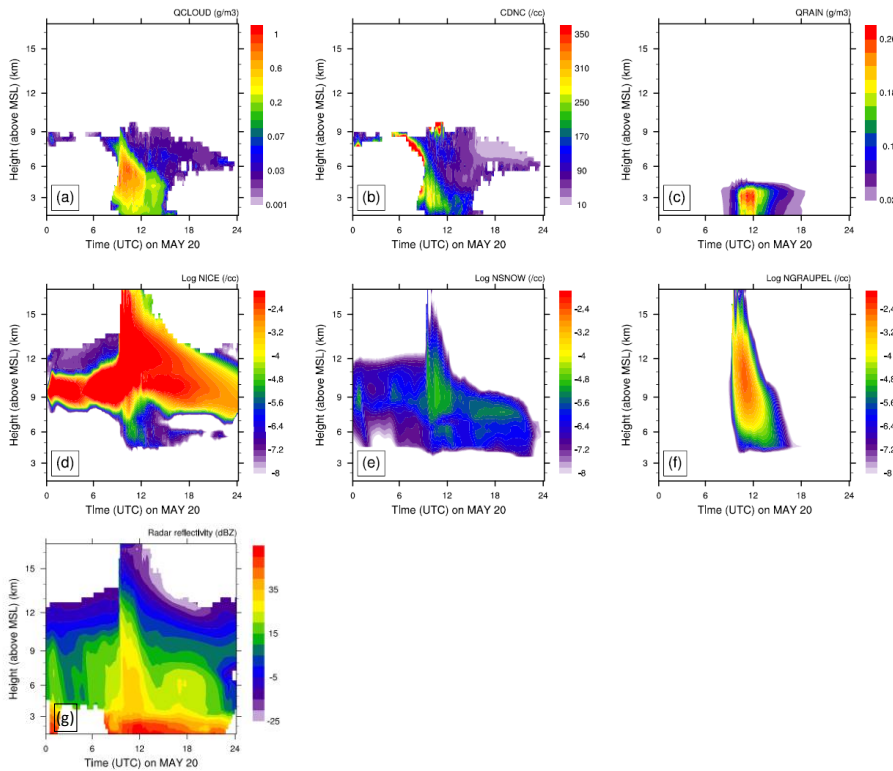


Figure 3: Time-height contours of domain averaged a) cloud water mixing ratio (QCLOUD); b) cloud droplet number concentration (CDNC); c) rainwater mixing ratio (QRAIN); d) number concentration of cloud ice (NICE); e) number concentration of snow (NSNOW); f) number concentration of graupel (NGRAUPEL). Due to a wide range of values, the log values number concentrations are plotted. The surface height is ~ 500 m. The averaging was done for cloud points with $LWC > 0.001 \text{ gm}^{-3}$ or total water content (TWC) $> 10^{-6} \text{ gm}^{-3}$. Also shown is the time-height evolution of domain averaged (g) radar reflectivity.

The time-height map of simulated radar reflectivity during 20 May, unconditionally averaged over the whole domain is shown in Figure 3g. It shows the well-defined squall line passing over the domain from 1100 to 1500 UTC. The maximum of this domain-wide simulated reflectivity is around 40 dBZ (Fig. 3d) when deep convection was happening. The instantaneous maximum of reflectivity at any grid-point (not shown) was about 50 dBZ. At

Deleted: 2

Deleted: Figure 2 shows the time-height evolution of various liquid and ice cloud microphysical parameters derived from the control simulation conditionally averaged over cloudy regions. The maximum of the average cloud droplet number concentration was around 250 cm^{-3} . The liquid water content LWC was typically less than 0.5 g m^{-3} . The freezing level (0°C) was around 4.1 km above MSL. The deep convection began around 10 UTC, followed by intense precipitation around 11 UTC, and reached its peak around 12 UTC. The time-height evolution of cloud ice, snow, and graupel number concentrations shows maxima shortly before 12 UTC, which coincides with the time of peak precipitation. This suggests that the ice phase was important in precipitation formation.¶

Deleted: 2

Deleted: 2

742 other times, the average reflectivity was typical of the stratiform cloud of about 15 dBZ. The
743 cloud top height of the squall line decreases after 1400 UTC.

744

745

746 4.2. Model validation against coincident observations of the storm

747 The extended stratiform region of the squall line while in the vicinity of the SGP CF was
748 sampled by the Citation aircraft equipped with a full suite of cloud microphysical
749 instrumentation (Sec. 2). The aircraft started sampling the stratiform precipitation region at
750 around 1300 UTC and continued the observations at sub-freezing temperatures from 1335 to
751 1515 UTC. Occasionally, the aircraft encountered weak convective updrafts (< 6 m/s). The
752 aircraft actively avoided convection that was more vigorous than that. In this section, we
753 validate various microphysical and dynamical quantities from the control simulation against
754 aircraft and ground measurements. The control run includes all primary and SIP processes of
755 ice initiation. The vertical profiles shown here are an average of five ensemble runs.

756

757 Figure 4 compares the aircraft observations against predicted microphysical quantities, with
758 both the predictions and observations identically averaged, conditionally over convective ($6 >$
759 $|w| > 1$ m/s) and stratiform regions ($|w| < 1$ m/s). The simulated LWC decreases exponentially
760 with height above the cloud base. There is considerable scatter in observed LWC at each
761 level. The various degrees of dilution of sampled parts of the cloud can cause these
762 variations in LWC at a given altitude. The maximum simulated LWC of 0.5 gm^{-3} was
763 observed in the convective region at temperatures warmer than -5°C . In the convective region
764 around -5°C , the measured LWC is lower than the simulated LWC by a factor of 3. For the

Deleted: 3

Formatted: Superscript

766 stratiform region, simulated values of LWC are in adequate agreement with observations.
 767 Overall, the means of observed LWC are in acceptable agreement with the model results for
 768 convective as well as stratiform regions.

Deleted: good agreement

769

770 The vertical profiles of simulated and observed Cloud Drop Number Concentration (CDNC)
 771 (Fig. 4c and 4d) showed that CDNC was lower than 300 cm^{-3} . In the convective region, the
 772 measured CDNC is 40% lower than the simulated CDNC at 15°C . However, an adequate
 773 agreement between them is found around -5°C . For the stratiform region, simulated CDNC is
 774 much higher in the mixed-phase region. However, at a temperature warmer than 0°C the
 775 values of observed CDNC are in acceptable agreement with observations. The observed and
 776 simulated mean diameter of cloud droplets varied between 6 to $15\text{ }\mu\text{m}$ over height (Figures 4e
 777 and 4f). There are few points in the convective region e.g., around -5°C , where the observed
 778 cloud drop diameter is 50% lower than the simulated value. An adequate agreement between
 779 simulated and observed cloud drop diameter was found for the stratiform region. Overall, the
 780 predictions of average CDNC and cloud droplet diameter, in both convective and stratiform
 781 regions, show a fair agreement with observations.

Deleted: 3

Deleted: 3

Deleted: Overall, the mean values of CDNC simulated for convective and stratiform regions are in good agreement with observations....

Formatted: Superscript

Formatted: Superscript

Formatted: Superscript

Deleted: -

Deleted: 3e

Deleted: 3f

Formatted: Superscript

Deleted: good

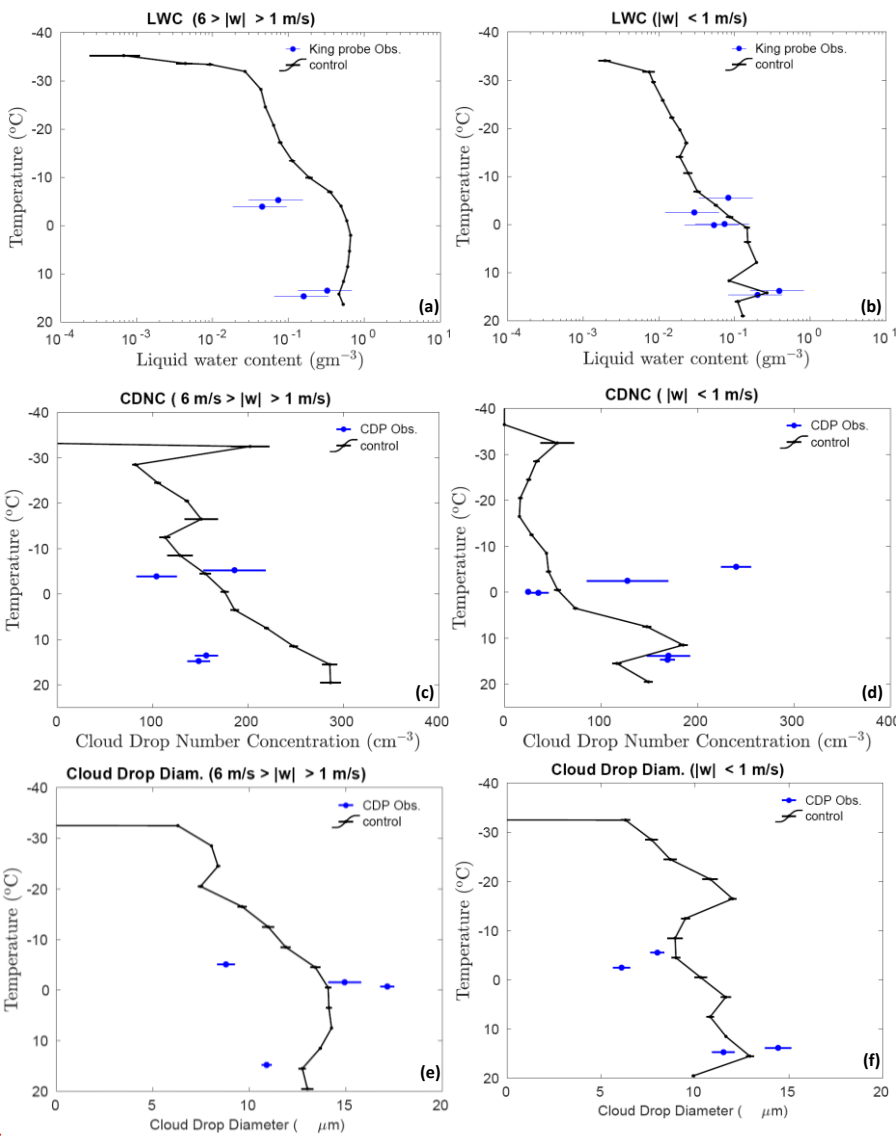
782

783 The ice particle number concentration from observations and the control simulation is also
 784 compared as shown in Figures 5a and 5b for convective and stratiform regions, respectively.
 785 It should be noted that the observed number concentration of ice particle particles smaller
 786 than $200\text{ }\mu\text{m}$ is prone to shattering, even with the use of the shattering correction algorithm.
 787 This can introduce a significant bias in the observed ice number concentration (Korolev et al.,
 788 1991). To avoid these biases, we have compared the number concentration of ice particles
 789 with a diameter greater than $200\text{ }\mu\text{m}$ from both observation and model (denoted by 'NT200').

800 However, in the rest of the manuscript (in sensitivity studies), the number concentration from
801 the model included ice particles of all size ranges.

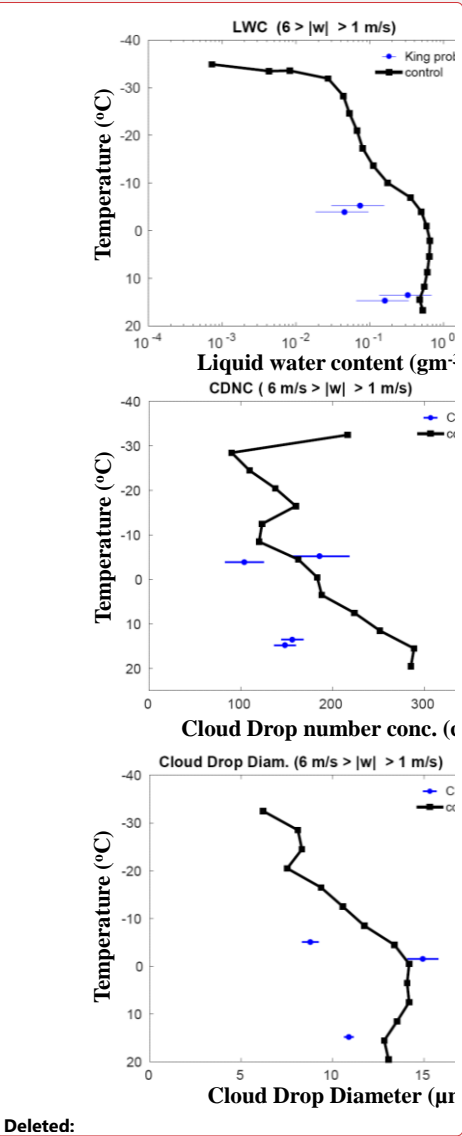
802

803



804

Deleted: ¶



Deleted:

807 **Figure 4:** Comparison of the control simulations by AC with aircraft observations, for liquid
 808 water content conditionally averaged over (a) convective ($6 \text{ m/s} > |w| > 1 \text{ m/s}$) and (b)
 809 stratiform ($|w| < 1 \text{ m/s}$) regions; cloud drop number concentration over (c) convective and (d)
 810 stratiform regions; average size of cloud droplets ($< 20 \mu\text{m}$) conditionally averaged over (e)
 811 convective and (f) stratiform regions. All the vertical profiles shown here are averaged for the
 812 whole domain. The error bars were estimated based on five ensemble runs.

Deleted: 3

814 Observations show that the concentration of ice particles gradually increases as the
 815 temperature decreases, as expected. The maximum ice number concentration from the aircraft
 816 observations (with $D > 200 \mu\text{m}$) is $\sim 0.06 \text{ cm}^{-3}$ around -15°C . Good agreement to within 50%
 817 at most levels, was found between the model simulated NT200 and that observed for the
 818 convective region.

Moved (insertion) [3]

Deleted: The ice particle number concentration from observations and the control simulation is also compared as shown in Figures 4a and 4b for convective and stratiform regions, respectively. It should be noted that the observed number concentration of ice particle particles smaller than $200 \mu\text{m}$ is prone to shattering, even with the use of the shattering correction algorithm. This can introduce a significant bias in the observed ice number concentration. To avoid these biases, we have compared the number concentration of ice particles with a diameter greater than $200 \mu\text{m}$ from both observation and model. However, in the rest of the manuscript, the number concentration from the model included ice particles of all size range. The number concentrations of ice particles from the model with a diameter larger than $200 \mu\text{m}$ (cloud ice, snow, graupel) (denoted by 'NT200') is compared with observed ice number concentrations from CIP as well as from combined probes including 2DC, CIP, and HVPS. Ice particles smaller than $200 \mu\text{m}$ from these imaging probes were excluded due to difficulties in measuring small ice particles (Korolev et al., 1991) as well as to avoid contamination from large cloud droplets. Observations show that the concentration of ice

Deleted: predicted

Moved up [3]: The number concentrations of ice particles from the model with a diameter larger than $200 \mu\text{m}$ (cloud ice, snow, graupel) (denoted by 'NT200') is compared with observed ice number concentrations from CIP as well as from combined probes including 2DC, CIP, and HVPS. Ice particles smaller than $200 \mu\text{m}$ from these imaging probes were excluded due to difficulties in measuring small ice particles (Korolev et al., 1991) as well as to avoid contamination from large cloud droplets. G

Deleted: 60 L

Deleted: ¹

Deleted: (

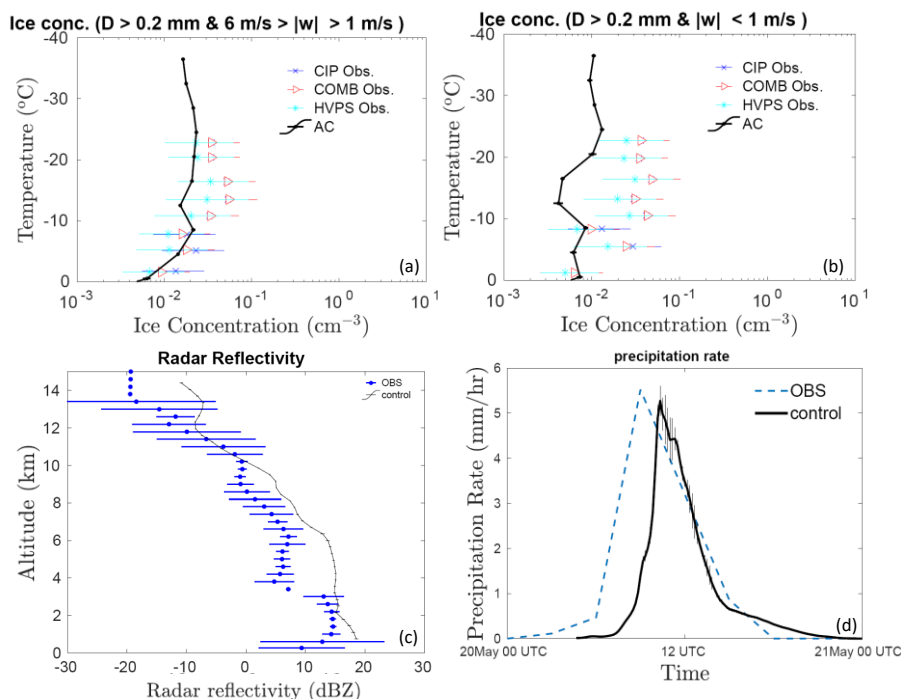
Deleted:)

Deleted: two-thirds of

Deleted: measured

819
 820 In the stratiform region, at most levels, model values of NT200 have the same order of
 821 magnitude as observations. However, between about the -10 and -16°C levels, the stratiform
 822 NT200 values are about half an order of magnitude lower than the observations. In similar
 823 simulations of the 20 May case, Fan et al. (2015) and Fridlind et al. (2017) also showed
 824 underestimation of simulated ice number concentrations. Compared to observations, their
 825 simulations showed half an order of magnitude bias in ice crystal number concentration.
 826 Comparatively, for the convective region, our model predicted ice number concentrations
 827 were in better agreement with observations. As mentioned in section 2.2, imaging probe data
 828 is prone to shattering, and various corrections were used to rectify it. However, there are
 829 currently no ways to determine how many undetected artifacts remain after shattering
 830 corrections have been applied (Baumgardner et al. 2022). Such uncertainties in measured ice
 831 number concentration could result in such bias in observed and simulated ice number
 832 concentrations. In summary, though the AC model is not totally perfect, it did a fair job in
 833 simulating observed ice number concentrations.

873



874

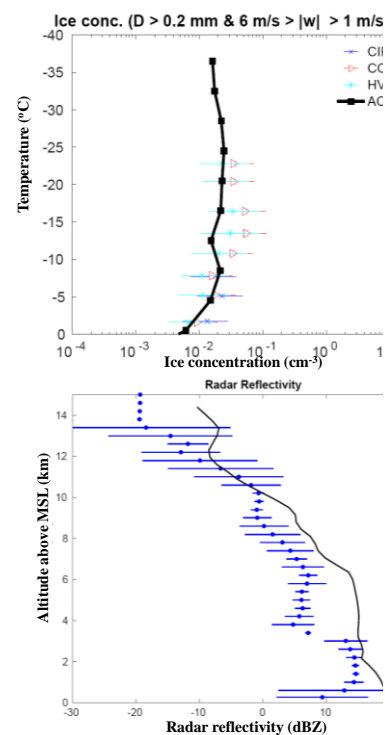
875

876 **Figure 5:** Comparison of the control simulations by AC with aircraft observations, for ice
 877 number concentration of all particles > 0.2 (NT200) mm in the maximum dimension of all
 878 microphysical species (cloud ice, graupel/hail, snow), averaged over (a) convective (6 m/s >
 879 |w| > 1 m/s) and (b) stratiform (|w| < 1 m/s) regions. (c) The vertical profile of simulated
 880 radar reflectivity conditionally averaged over all regions of significant reflectivity (> -20
 881 dBZ) at each level is compared with observations from ground-based radars. The temperature
 882 corresponding to each altitude is mentioned on the right axes; (d) predicted precipitation rate
 883 (mm/hr) compared with ground observations at the SGP CF. All the vertical profiles shown
 884 here are averaged for the whole domain. The error bars were estimated based on five
 885 ensemble runs.

886

887

888 In Figure 5c, the radar reflectivity from vertically pointing Ka-band ARM zenith radar is
 889 compared with the mean profile from model simulations. This figure illustrates that simulated
 890 reflectivity profiles below roughly 3 km and above 8 km MSL altitudes are in good



Deleted:

Deleted: 4

Deleted: 4

Deleted: illustrates

895 agreement with observations. Between 3 and 8 km MSL (temperatures of 2 and -30°C), the
896 bias in reflectivity from model simulations and observations is about 10 dBZ. Thus, the
897 simulated reflectivity is substantially higher than observed, particularly at levels where the
898 aircraft sampled the clouds. Fridlind et al. (2017), as well as Fan et al. (2015), noticed similar
899 overestimations of reflectivity within stratiform outflow of the squall line case on 20 May.
900 They attributed the reflectivity biases to significantly larger ice particles in the simulations
901 than observed.

Deleted: 7-8

902
903 Figure 5d compares the time series of precipitation rate from the control simulation with the
904 radar-based precipitation estimates. In both, control simulation and observations, a maximum
905 precipitation rate of about 5 mm/hr was noticed, with an error in the prediction of less than
906 5%. In comparison to observations, the simulated squall line arrives 1-2 hours later. The lack
907 of resolution of the 3D turbulence in the planetary Boundary Layer and uncertainties
908 associated with the 3D structure of initial and boundary conditions can all have an
909 independent impact on the simulated rainfall structure, resulting in a delayed peak.
910 Nonetheless, AC has done a fair job in simulating the peak in the predicted precipitation rate.

Deleted: 4

Deleted: PBL

Deleted: good agreement

Deleted: between predicted and retrieved precipitation rates is observed. ¶

912 4.3 Analysis of simulation with ice particle budgets and tagging tracers

913 The activated PBAP INPs from the control run are shown in Figure 6 for the convective and
914 stratiform regions. In addition to the PBAP INPs, Figure 6 also shows the activated INPs
915 from dust and black carbon. It should be noted that these concentrations shown here are based
916 on advective tagging tracers that follow the diffusion, ascent, and descent inside cloud
917 motions. Overall, bacterial, and fungal particles dominate the biological INP concentration in

Deleted: PBAP

Deleted:

Deleted: budget of the

Deleted: 5

the simulated cloud. For example, at -20°C the activated INPs from bacteria and fungi are higher than the other three groups of **PBAP** INPs (detritus, pollen, algal) by two orders of magnitude in both convective as well as stratiform regions. At that level in convective regions, the average concentration of simulated active **PBAP** INPs is about $3 \times 10^{-6} \text{ cm}^{-3}$, which is two orders of magnitude less than the maximum total for all active INPs (about $3 \times 10^{-4} \text{ cm}^{-3}$) in the whole simulation. Overall, the predicted total INP concentration is dominated by black carbon and dust. At -10°C, the Activated INPs from dust and black carbon differ by an order of magnitude from the total **PBAP** INPs in convection.

Deleted: PBAP

Deleted: the maximum of

Deleted: PBAP

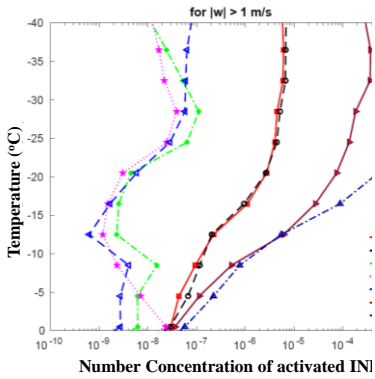
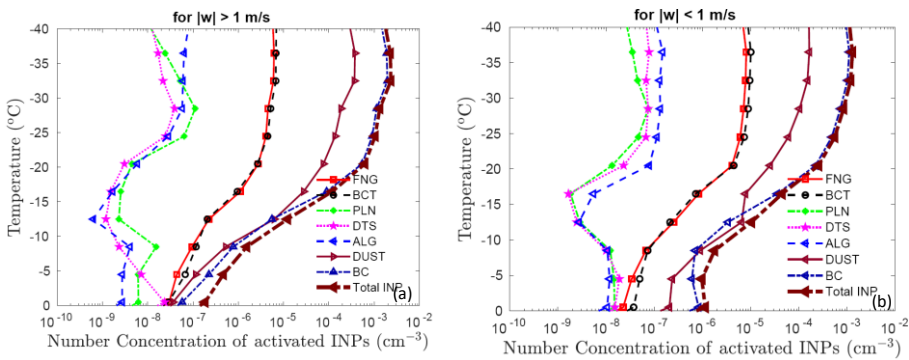
Deleted: 0.003 L-1

Deleted: 0.3 L-1

Deleted: In addition to the PBAPPBAP INPs, Figure 5 also shows the activated INPs from dust and black carbon. ...

Formatted: Superscript

Deleted: PBAP



Deleted:

Figure 6: The activated number concentration INPs from various **PBAP** groups along with dust (DUST) and black carbon (BC) and total INPs at various temperatures for (a) convective and (b) stratiform regions. All the vertical profiles shown here are averaged for the whole domain.

Deleted: 5

Deleted: PBAP

The formation of ice in a cloud is a result of several primary and secondary processes. It is important to understand the relative importance of these processes in precipitation formation. To that end, Figure 7a shows the ice particles initiated from various sources throughout the 3D domain of the entire simulation.

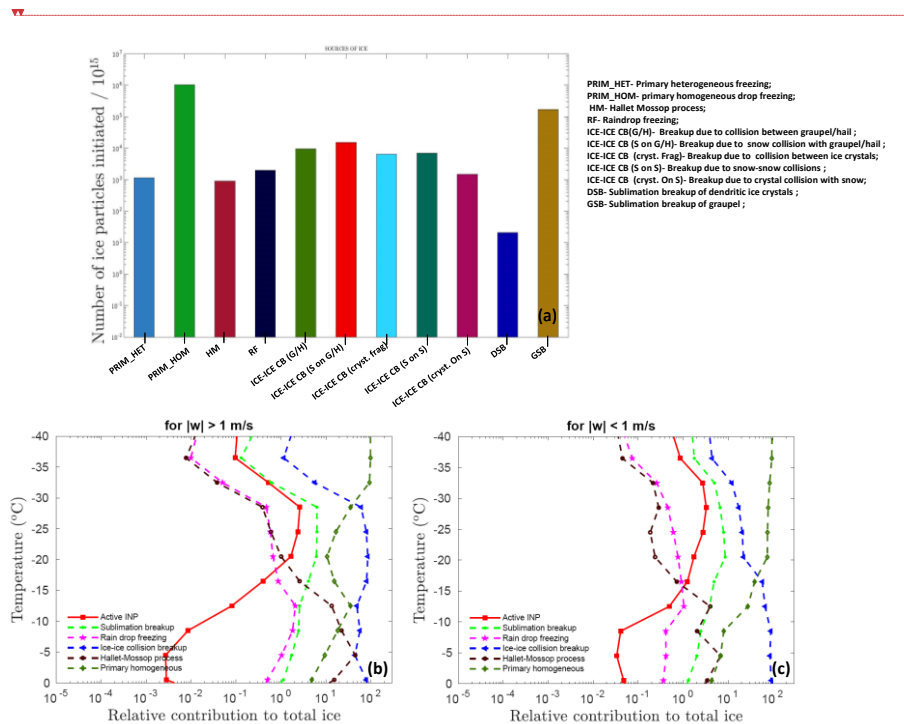
Deleted: in

Deleted: 6a a budget is provided for the

Deleted: total numbers of all

Deleted:

963



964

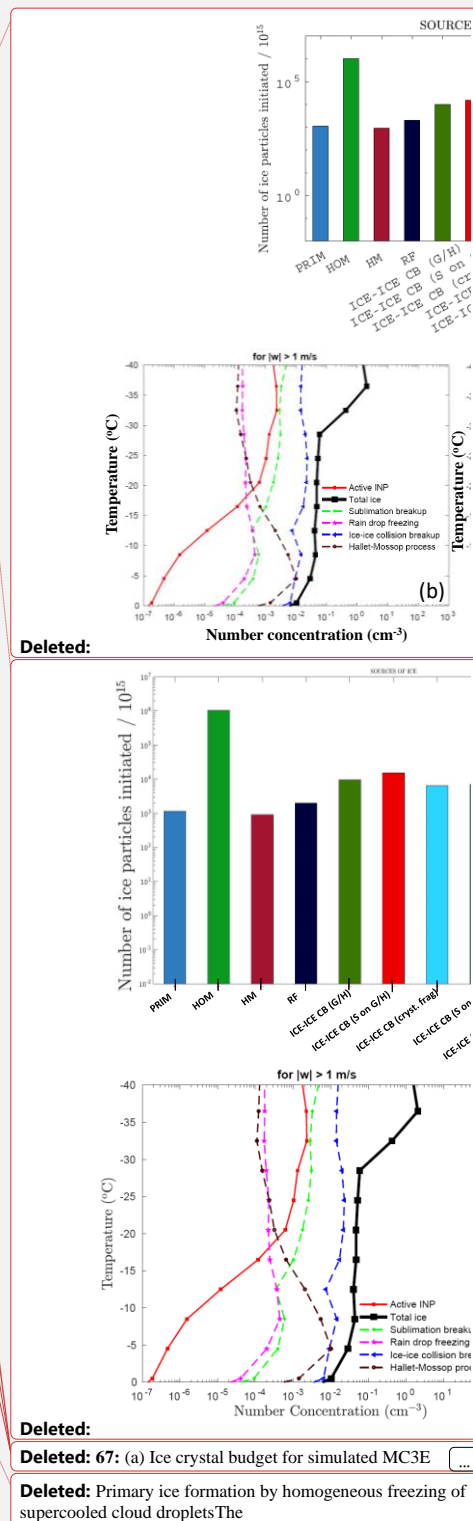
965

966 **Figure 7:** (a) Ice crystal budget for simulated MC3E case. The number of ice crystals
 967 produced by various mechanisms (as shown in the legend box) per 10¹⁵ particles is shown.
 968 Also shown is the relative contribution of various SIP mechanisms such as sublimation
 969 breakup, raindrop freezing, ice-ice collision breakup, and the Hallett-Mossop process to the
 970 total ice number concentration as a function of temperature, averaged conditionally over only
 971 (b) convective and (c) stratiform regions. The relative contribution was calculated based on
 972 advective tagging tracers for the given process. The convective and stratiform regions were
 973 identified based on criteria $|w| > 1$ and $|w| < 1$, respectively.

974

975

976 The primary homogeneous (PRIM HOM) dominates the total ice budget. Among all SIP
 977 mechanisms, breakup caused by collisions between various ice particles is the most important
 978 in determining total ice number concentration. The ice production by sublimation breakup of



Deleted: 67: (a) Ice crystal budget for simulated MC3E
 Deleted: Primary ice formation by homogeneous freezing of
 supercooled cloud dropletsThe

998 graupel is slightly lower than PRIM HOM. However, the contribution of ice production via
 999 sublimation breakup of dendritic ice crystals is negligible.

1000

1001 Figure 7b and 7c depict the relative importance of ice concentration from various SIP
 1002 mechanisms, as well as active INPs in determining total ice number as a function of
 1003 temperature for convective and stratiform regions. Each source of ice displayed is tracked
 1004 with advective “tagging tracers” throughout the simulation. Overall, at temperatures warmer
 1005 than -15°C, the contribution to the total ice number concentration from various SIP is 2-3
 1006 orders of magnitude higher than the concentration of active INPs, highlighting the importance
 1007 of SIP mechanisms in ice formation. At -25°C, breakup in ice-ice collisions contributes
 1008 around 75% and 20% of the total ice concentration in the convective and stratiform regions,
 1009 respectively. At the same temperature, in both convective and stratiform regions, sublimation
 1010 breakup and raindrop freezing contribute about 8% and 0.8%, respectively. It can be
 1011 observed that in the convective regions at temperatures warmer than -30°C, SIP mechanisms
 1012 are important in determining the total ice concentrations, whereas at colder temperatures
 1013 homogeneous nucleation is dominant. In the stratiform region, this crossover occurs at a
 1014 much warmer temperature around -18°C. At temperatures colder than this homogeneous
 1015 nucleation is a major contributor to the total ice whereas at warmer temperatures SIP
 1016 mechanisms prevail. Overall, the contribution of active INP to the total ice is lower than 3%.

1017

1018 Secondary ice formation via the HM process of rime-splintering contributes significantly to
 1019 ice production at temperatures warmer than about -15 °C (Fig. 7b and 7c), enhancing the ice
 1020 concentration beyond the primary ice. In the convective region, the contribution of the HM
 1021 process in total ice can reach as high as 40% around -5°C. The simulated cloud droplet

Deleted: homogeneous freezing

Deleted: 6b

Deleted: s

Deleted: dependency on the ambient temperature of components of ice concentration from

Deleted: and total ice number concentration

Deleted: 30

Deleted: 1

Deleted: 2

Deleted: 50

Deleted: 10

Deleted: for

Deleted: 7

Deleted: 5

Formatted: Superscript

Formatted: Superscript

Deleted: 6

Deleted: b

Deleted: In the convective region, the contribution of this process to the total ice concentration is maximum around -5°C (about 30%). ...

diameter is mostly smaller than 15 μm . It is smaller than the cloud droplet size required for the HM process to occur. In AC, the rate of the rim-splintering mechanism depends on the concentration of droplets > 24 μm . It should be noted that in the AC model HM process is treated with a factor multiplying the fragment emission which depends on the cloud droplet size. This factor is zero for cloud diameter below 16 μm and unity above 24 μm with linearly interpolated in between.

1047

1048 5. Results from sensitivity tests about the influence of PBAP

1049 To quantify the effect of multiple types of PBAPs on cloud properties, sensitivity tests were
1050 performed by modifying the control simulation and comparing the perturbed simulations with
1051 it.

1052 **Table 3:** Description of various sensitivity simulations carried out in the current study. The
1053 corresponding figures for each simulation are also mentioned.

1054

Simulation	PBAP included	Changes in initial PBAP mass	Cloud processes switched on/off	Corresponding figures
control (five ensembles)	ALL PBAPs act as CCN and INP	-	All cloud processes in the AC are on	Figures 4 onward all
no-PBAP (five ensembles)	No PBAP can act as CCN and INP	All PBAPs mass was set to zero	Same as control	Figures 8, 9, 10, 11, 12
no-PBAP INP (five ensembles)	No PBAP can act as INP (CCN activity of PBAP is on)	-	Same as control	Figures 8, 9, 10, 11, 12
high-PBAP (five ensembles)	Same as control	All PBAPs mass was	Same as control	Figures 8, 9, 10, 11, 12

Deleted: represents the observed dependency of

Deleted: The fluctuations in CCN concentration in the boundary layer can result in larger cloud droplet diameters in some parts of the cloud, favouring secondary ice formation via the HM process. It

Deleted: from

Deleted: PBAP

Deleted: PBAPs

Deleted: studies

Formatted: Font: 8 pt

Formatted: Font: 8 pt

Formatted Table

Formatted: Font: 8 pt

Formatted: Font: 8 pt

Deleted: C

Deleted: s

Formatted: Font: 8 pt

Formatted: Font: 8 pt

Formatted: Font: 8 pt

Deleted: 3, 4, 7, 8, 9, 10, 13, 14, 15

Deleted: -

Formatted: Font: 8 pt

Formatted: Font: 8 pt

Deleted: 7, 8, 9, 10

Formatted: Font: 8 pt

Formatted: Font: 8 pt

Formatted: Font: 8 pt

Formatted: Font: 8 pt

Formatted: Font: 8 pt

Deleted: 7, 8, 9, 10

Formatted: Font: 8 pt

Formatted: Font: 8 pt

Formatted: Font: 8 pt

Formatted: Font: 8 pt

Deleted: 7, 8, 9, 10

Formatted: Font: 8 pt

		boosted by a factor of 10		
very high-PBAP (five ensembles)	Same as control	All PBAP mass boosted by a factor of 100	Same as control	Figures 8, 9, 10, 11, 12
ultra high-PBAP (five ensembles)	Same as control	All PBAP mass boosted by a factor of 1000	Same as control	Figure 8, 9
no-sublimation breakup	Same as control	-	SIP from sublimation breakup is off	Figure 13
No-collisional ice-ice breakup	Same as control	-	SIP from the collision between ice particles is off	Figure 13
No-secondary	Same as control		ALL SIP mechanisms are off	Figures 13, 14
very high-PBAP with no secondary	Same as control	All PBAP mass boosted by a factor of 100	ALL SIP mechanisms are off	Figure 14

Formatted: Font: 8 pt

Formatted: Font: 8 pt

Deleted: 7, 8, 9, 10

Formatted: Font: 8 pt

Deleted: 9

Formatted: Font: 8 pt

Formatted: Font: 8 pt

Formatted: Font: 8 pt

Deleted: no-fng

Deleted: 14

Formatted: Font: 8 pt

Formatted: Font: 8 pt

Deleted: 14

Formatted: Font: 8 pt

Deleted: 14, 15

Formatted: Font: 8 pt

Deleted: 15

Formatted: Font: 8 pt

Formatted: Font: 8 pt

Formatted: Font: 8 pt

Formatted: Indent: First line: 0 cm

Simulations were performed by eliminating all PBAPs from the control ('no-PBAP' case) and by multiplying their initial loadings at all levels by factors of 10 and 100 ('high-PBAP' and 'very high-PBAP' cases) respectively. Comparison with the control simulation reveals the overall effect from both the CCN and IN activities of all bioaerosols combined. These factors are justified by considering the variations in PBAP concentrations in the range of about 0.1 to 30 L⁻¹ over North American forests (Huffman et al. 2013). An additional simulation was conducted with a 1000-fold increase in initial PBAP loading ('ultra high-PBAP') to investigate if these unrealistically high concentrations of PBAPs could affect the ice phase in a purely hypothetical scenario. Five ensemble runs were carried out for all major simulations

Deleted: <#>All PBAPsPBAP¶

Deleted: PBAPs

Deleted: pbap

Deleted: pbap

Deleted: pbap

Deleted: PBAP

Deleted:

Deleted: PBAP

Deleted: pbap

Deleted: PBAPs

1098 involving perturbations in PBAP loading. The ensemble runs were carried out by varying the
1099 perturbation in initial conditions (water vapor mixing ratio).

1100
1101 Additional simulations were performed by removing treatment of biological IN activity in the
1102 EP ('no-PBAP INP' case) relative to the control run. A comparison of both additional
1103 simulations against the corresponding simulations with the full change in the PBAP loadings
1104 (no-PBAP and high-PBAP cases) reveals the separate roles of the INP and CCN activities for
1105 the changes in biological material. Apart from these changes in PBAPs, the perturbed
1106 simulations are identical to the control run.

1107
1108 Figure 8 reveals the effects of all bioaerosols on cloud properties in the convective region
1109 (/w/ > 1 m/s). Overall, changes in cloud microphysical properties including liquid water
1110 content, cloud droplet size, cloud drop number concentration, ice number concentration are
1111 less sensitive to the changes in PBAPs for the convective part of the simulated clouds and are
1112 not statistically significant. The LWC, cloud droplet number and cloud drop diameter in the
1113 perturbed simulations does not differ much (< 3%) from the control run. For the whole storm,
1114 considerable changes in the spatial distribution of total ice number concentration are observed
1115 due to changes in PBAPs (see Figure S5). However, vertical profiles showed very small
1116 changes in the ice number concentrations. In the convective region, changes in ice crystal
1117 number concentration due to changes in PBAPs are negligible (< 6%). This includes the
1118 extreme changes in bioaerosol loading (ultra high-PBAP case).

Deleted: pbap

Deleted: Comparison

Deleted: PBAP

Deleted: pbap

Deleted: pbap

Deleted: PBAPs

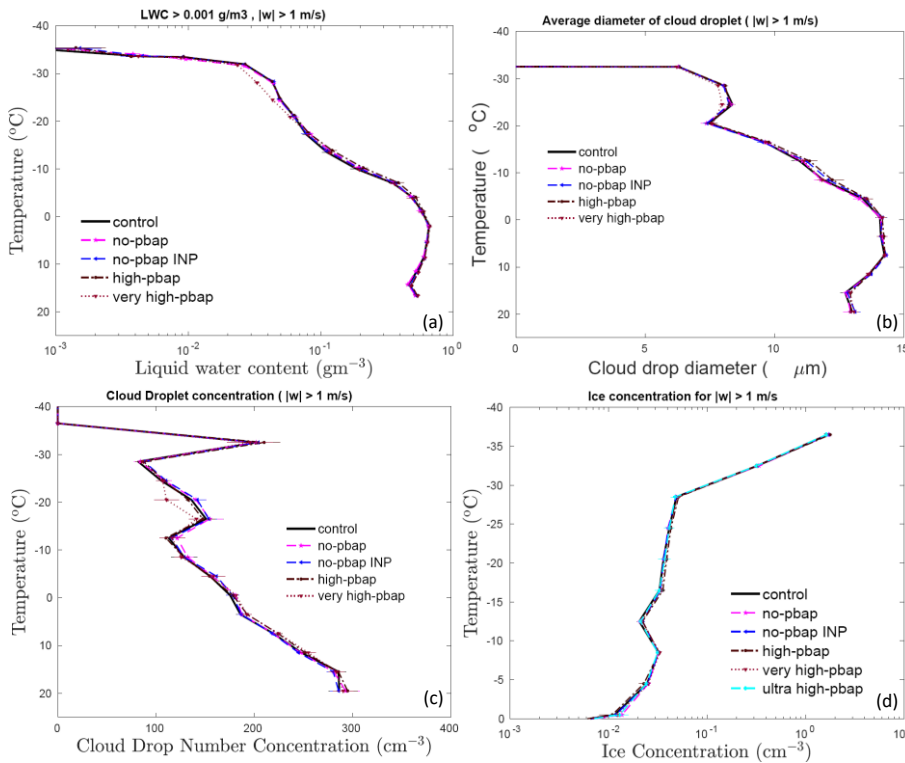
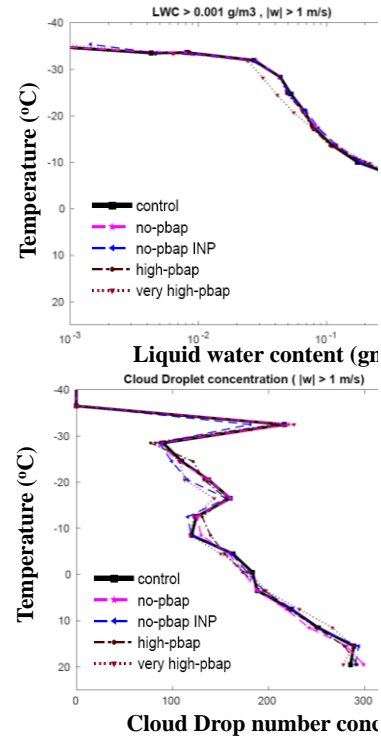


Figure 8: The temperature dependence of the (a) liquid water content, the (b) cloud droplet number, (c) the cloud droplet diameter, and the (d) total ice number concentration for 'control' simulation and various sensitivity runs involving a change in total **PBAP** number concentrations for in the convective region. The averaging conditions are mentioned at the top of each figure. The ice number concentration from the ultra high-**PBAP** is also shown in panel d. All the vertical profiles shown here are averaged for the whole domain.



Deleted:

Deleted: 7

Deleted: PBAP

Deleted: pbap

1140

1141

Table 4: Changes in mean cloud macro and microphysical properties associated with various sensitivity tests carried out.**Formatted:** Font: Bold**Formatted:** Width: 29,7 cm, Height: 21 cm, Header distance from edge: 1,25 cm, Footer distance from edge: 1,25 cm

<u>Simulations</u>	<u>Ice number conc. (cm⁻³)</u>			<u>LWC (g/m³)</u>			<u>Downward</u> <u>shortwave</u> <u>radiation flux</u>	<u>Downward</u> <u>longwave</u> <u>radiation flux</u>	<u>Cloud cover (%)</u>	<u>Accumulated</u> <u>surface</u> <u>precipitation</u> <u>(mm)</u>
	<u>Total</u>	<u>Convective</u>	<u>Stratiform</u>	<u>Total</u>	<u>Convective</u>	<u>Stratiform</u>				
<u>control</u>	0.76	0.47	0.052	0.128	0.285	0.063	165.28	136.8	0.231	20.10
<u>no-PBAP</u>	0.72	0.46	0.057	0.13	0.281	0.069	163.42	139.6	0.224	19.92
<u>no-PBAP INP</u>	0.80	0.48	0.053	0.13	0.287	0.068	164.7	137.3	0.229	20.14
<u>high-PBAP</u>	0.71	0.44	0.050	0.14	0.30	0.068	168.1	138.6	0.227	19.96
<u>very high-PBAP</u>	0.73	0.44	0.043	0.135	0.29	0.068	166.07	138.8	0.24	20.04
<u>ultra high-PBAP</u>	0.60	0.48	0.03	0.141	0.29	0.070	159.4	133.1	0.26	20.70
<u>no-sublimation</u> <u>breakup</u>	0.84	0.52	0.054	0.12	0.26	0.065	184.1	144.9	0.21	20.52
<u>No-collisional ice-ice</u> <u>breakup</u>	1.82	1.35	0.21	0.15	0.32	0.082	153.4	123.6	0.24	15.41
<u>No-secondary</u>	1.89	1.45	0.18	0.15	0.30	0.08	158.6	115.7	0.26	24.23
<u>very high-PBAP with</u> <u>no secondary</u>	1.85	1.38	0.20		0.30	0.085	208.3	127.8	0.28	23.95

Figure 9 shows the corresponding effects in the stratiform region ($w < 1$ m/s) from all bioaerosols. The changes in warm microphysical properties as a result of changes in PBAP loadings are smaller than 10%. In this part of the cloud, the ice-microphysical parameters are comparatively more sensitive to the changes in PBAP than in the convective region. The ultra high-pbap case predicted ~40% lower ice number concentration than the control run. However, these changes in ice number concentration are not significant as the error bars associated with ensemble members overlap. For the stratiform region, all other simulations considered here showed < 10% change in ice number concentrations compared to the control run. These changes in ice number concentration due to PBAPs are mostly controlled through their effect on homogeneous freezing above the -36°C level as shown in Figure 9e by tagging tracer for homogeneous nucleation. These ice particles can then advect to lower levels affecting ice number concentrations in the mixed-phase region.

Figure 10 shows the number of ice particles generated by homogeneous nucleation, various mechanisms of primary nucleation (10a), and secondary ice production (10b) per 10^{15} ice particles for the entire storm. Homogeneous freezing dominates the ice production among the three broad types of ice formation mechanisms (heterogeneous and homogeneous ice nucleation, SIP). The maximum changes in ice nucleated through the primary ice mechanism are noticed for the very high-PBAP case and can be attributed to the 100-fold increase in all PBAP loading. The very high-PBAP simulation predicted a 15% lower number of homogeneously nucleated ice than the control run. The very high-PBAP cases predicted about 80% more primary ice crystals formed at temperatures warmer than -30°C. At temperatures colder than -30°C, this case predicted 20% more primary ice crystals than the control run. The very high pbap case showed an increase in primary heterogeneous ice and a decrease in primary homogenous ice. Since the contribution of primary homogenous ice

Deleted: Figure 7 reveals the effects of all bioaerosols on cloud properties in the convective region ($w > 1$ m/s). Overall, changes in cloud microphysical properties including liquid water content, cloud droplet size, cloud drop number concentration, ice number concentration are less sensitive to the changes in PBAPsPBAP for the convective part of the simulated clouds than the stratiform part (Figure 9). The maximum change in simulated LWC is noted in the very-high pbapPBAP simulation at -25°C and is less than 50% as compared to the control. The cloud droplet number and cloud drop diameter in the perturbed simulations does not differ much (< 5%) from the control run. In the convective region, changes in ice crystal number concentration due to changes in PBAPsPBAP are negligible. This includes the extreme changes in bioaerosol loading (ultra high-pbapPBAP case).¶

Deleted: PBAP

Deleted: very

Deleted: PBAPs

Deleted: no-pbapPBAP

Deleted: INP

Deleted: a

Deleted: 6

Deleted: higher

Deleted: at -20°C

Deleted:

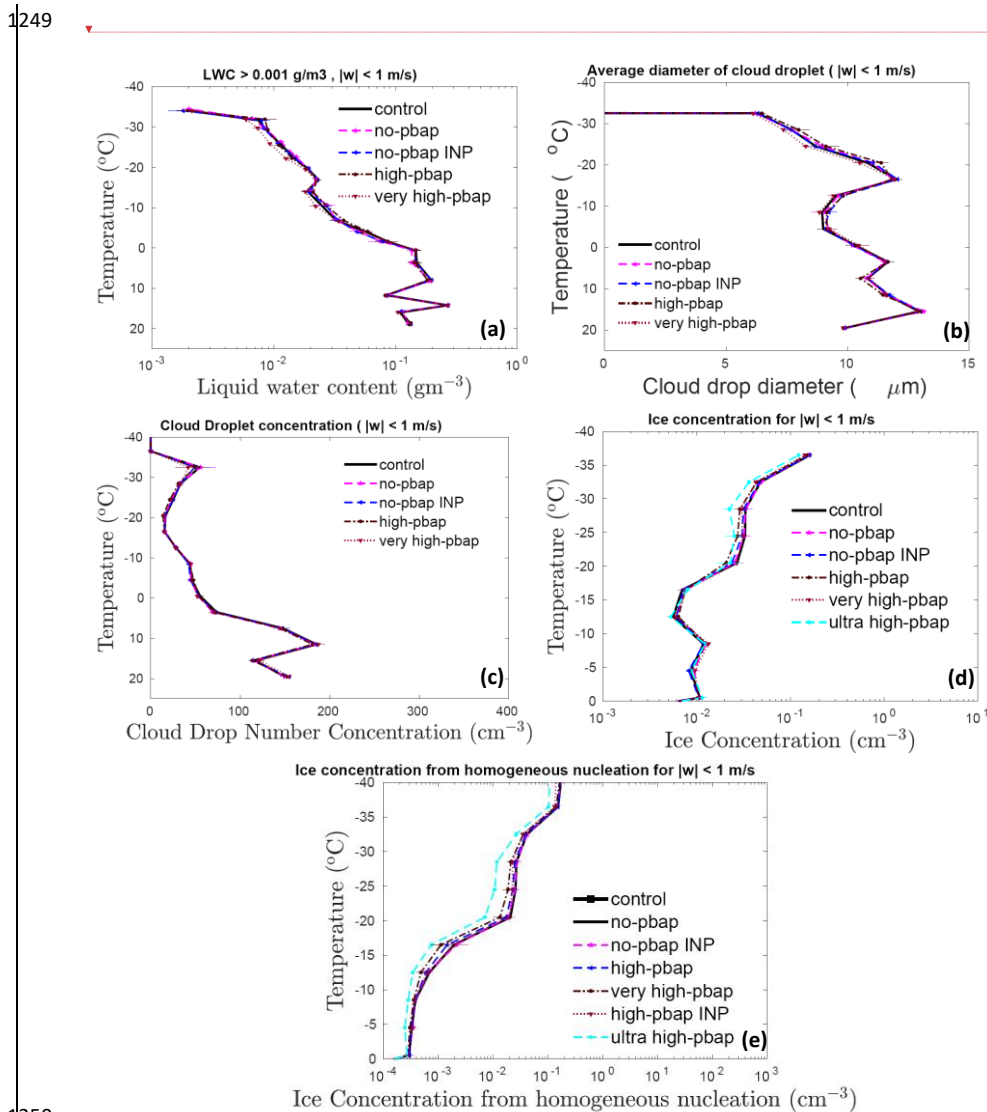
Deleted: is could be associated with enhanced ice formation

Deleted: nucleation

Formatted: Superscript

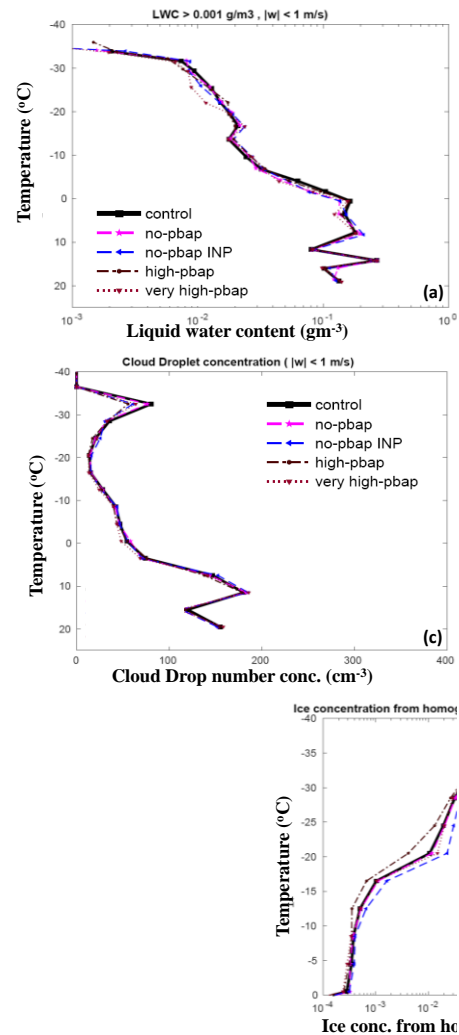
Deleted: since the cloud droplet number concentration at this level was slightly higher compared to the control run. At this temperature level, the changes in ice number

1245 nucleation is much higher in determining the total ice number concentration when compared
 1246 with primary homogeneous nucleation, the overall effect of the very high pbap case is a
 1247 decrease in total ice number concentration as shown in Figure 9 and Table 4.



Deleted: ¶

Figure 9e shows that at the colder temperatures ($T < -20^{\circ}\text{C}$) homogeneous freezing aloft with downwelling of homogeneously nucleated ice dominates the ice number in all simulations. The sensitivity of ice number concentrations to PBAPPBAP loading at temperatures colder than ¶

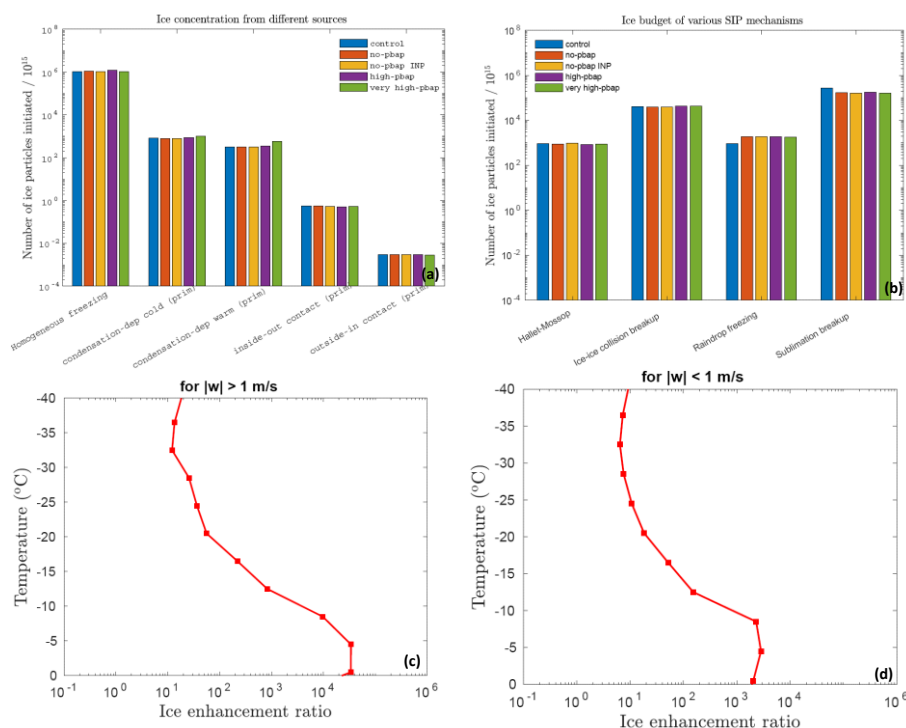


1250

1259 **Figure 9:** The temperature dependence of (a) the liquid water content, (b) the cloud droplet
 1260 number, (c) the cloud droplet diameter, and the (d) total ice number concentration for
 1261 ‘control’ simulation and various sensitivity runs involving a change in total **PBAP** number
 1262 concentrations for in the stratiform region. Also shown is the temperature dependence of (e)
 1263 ice concentration from homogeneous freezing. The averaging conditions are mentioned at the
 1264 top of each figure. The **total ice number concentration and ice number from homogeneous**
 1265 **freezing from ultra high-PBAP are also shown in panels d and e.** All the vertical profiles
 1266 shown here are averaged for the whole domain. **The error bars are based in ensemble runs.**

1267

1268



1269

1270 **Figure 10:** The number of ice crystals produced during the whole storm by (a) primary ice
 1271 nucleation mechanisms and homogeneous freezing as well as (b) various SIP mechanisms (as
 1272 shown in the legend box) per 10^{15} particles is shown for various sensitivity runs.

1273

1274

1275 Figure 10b shows that among SIP mechanisms, the contributions of ice-ice collision breakup
 1276 and sublimation breakup are higher by an order of magnitude than the HM process and

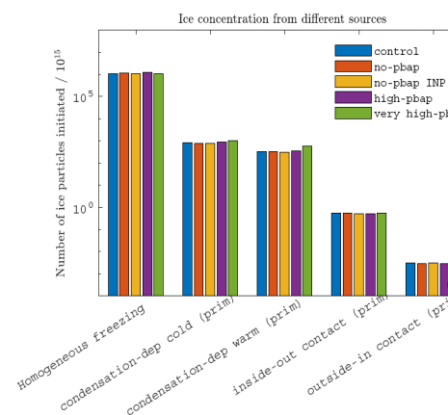
Deleted: PBAP

Deleted: ultra

Deleted: pbap

Deleted: is

Deleted: -20°C is mostly associated with homogeneously nucleated ice downwelled in the mixed-phase from above. At temperatures warmer than -15°C the predicted ice number concentrations are less sensitive to the changes in bioaerosol loading. The biggest change was predicted for the very high-pbapPBAP case, which had a 20% lower ice number concentration than the control run. The changes in snow and graupel mass (including warm and cold components) were lower than 10% (not shown here).



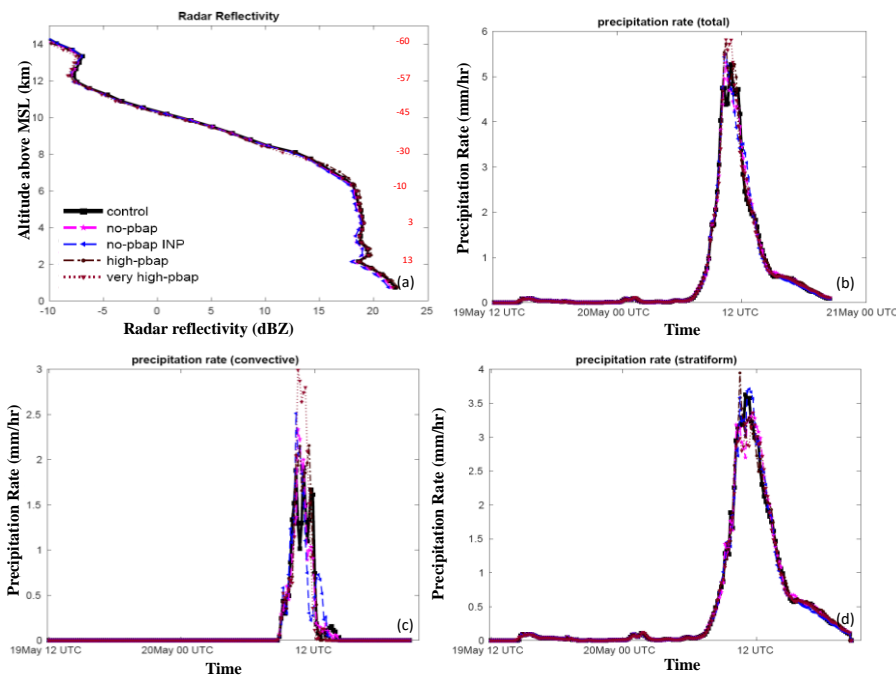
Deleted: Figure 10 shows the number of ice particles generated by homogeneous nucleation, various mechanisms of primary nucleation (10a), and secondary ice production (10b) per 10^{15} ice particles for the entire storm. Homogeneous freezing dominates the ice production among the three broad types of ice formation mechanisms (heterogeneous and homogeneous ice nucleation, SIP). The maximum changes in ice nucleated through the primary ice mechanism are noticed for the very high-pbapPBAP case and can be attributed to the 100-fold increase in all PBAPPBAP loading. The high-pbapPBAP simulation predicted a 15% higher number of homogeneously nucleated ice than the control run. The very high-pbapPBAP cases predicted about 80% more primary ice crystals formed at temperatures warmer than -30°C. At temperatures colder than -30°C, this case predicted 20% more primary ice crystals than the control run.

1308 raindrop fragmentation. However, the budget analysis (not shown in the plot) showed that
 1309 about 75% of the fragments associated with sublimation breakup are prone to evaporation,
 1310 making ice-ice collision breakup a major SIP mechanism. The estimated ice enhancement
 1311 ratio, which is a ratio between the number concentrations of total ice (excluding
 1312 homogeneous nucleation) and primary ice, is shown in Figures 10c and 10d for convective
 1313 and stratiform regions respectively. Overall, the ice enhancement ratio varied between 10 to
 1314 10^4 , which indicates the importance of SIP mechanisms. The budget analysis shows that
 1315 overall, the perturbations in bioaerosols resulted in very small changes (with maximum
 1316 change < 40%) in ice generated by SIP mechanisms.

Deleted: is two orders of magnitude

Formatted: Superscript

Deleted: 5



1317
 1318 **Figure 11:** The vertical profiles of (a) radar reflectivity are shown for simulations involving
 1319 changes in PBAP. (b) The temporal evolution of the total surface precipitation rate averaged
 1320 over the domain is also shown. The time series of surface precipitation rate averaged over the
 1321 domain is also shown separately for (c) convective and (d) stratiform regions. All the vertical
 1322 profiles shown here are averaged for the whole domain.

Deleted: PBAPs

1326 Figure 11a shows the effects of PBAP on the simulated radar reflectivity for the whole storm.
 1327 When compared to the control run, there is no significant difference in the simulated radar
 1328 reflectivity of the perturbed simulations (< 4%). Figure 11b depicts the sensitivity of the total
 1329 surface precipitation rate averaged over the domain to the changes in total PBAPs. As shown
 1330 in Figure 11b, the peak in surface precipitation rate is boosted by about 10% in the very high-
 1331 PBAP cases compared to the control run. In remaining perturbed simulations, changes in
 1332 surface precipitation rate are less than 5% when compared with the control run. The
 1333 contribution from the stratiform component of rain is higher in the total amount of rain (90%)
 1334 as compared to the convective rain (remaining 10%) (see Fig. 11c and 11d). Convective
 1335 rainfall is more sensitive to the changes in PBAPs than stratiform rainfall. The increase in
 1336 PBAPs by 100-fold results in a 50% higher peak of convective rainfall rate as compared to
 1337 the control run.

1338
 1339 The changes in accumulated surface precipitation due to PBAPs are shown in Table 4. The
 1340 spatial distribution of accumulated surface rainfall shows considerable variation associated
 1341 with changes in PBAPs (Figure S7). However, the overall effect of PBAPs on accumulated
 1342 surface precipitation is minimal (< 4%).

1343
 1344
 1345 Figure 12 shows the domain averaged vertical profiles of shortwave, longwave fluxes, and
 1346 cloud fractions for the different sensitivity tests considered here. Among all the sensitivity
 1347 runs, only the high-PBAP case showed a noticeable effect on shortwave flux, which was 2%
 1348 higher than the control run. The variations in longwave fluxes were less than 1%. The vertical
 1349 profiles of cloud fraction show that a 100-fold increase in total PBAPs results in a 10%
 1350 higher cloud fraction between 8 and 12 km. However, the overall change in cloud fraction

Deleted: ¶
¶

Deleted: PBAPs

Deleted: PBAPs

Deleted: Overall, PBAPsPBAP have a minimal effect on surface precipitationAs shown in Figure 11b

Deleted: , and it is most effective during the period when precipitation is at its highest. ...T
T

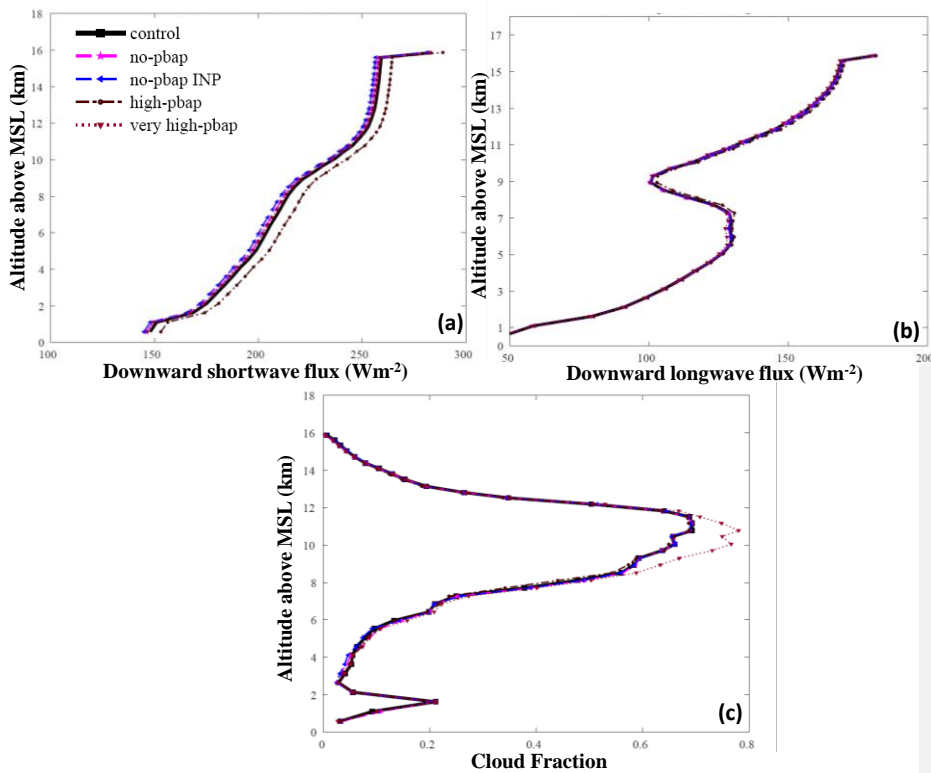
Deleted: T

Deleted: pbap

Deleted: PBAPs

Deleted: PBAPs

1364 from 100-fold increase in PBAP is less than 4% as shown in Table 4. The cloud fraction in
1365 other sensitivity runs was less sensitive to the changes in PBAP loadings. The ultra high-pbap
1366 case simulated a predicted 10% higher cloud fraction than the control run (see Table 4)
1367



1368
1369 **Figure 12:** The domain averaged vertical profiles of downward components of (a) shortwave
1370 flux, (b) longwave flux, and (c) cloud fraction for various sensitivity experiments. The data
1371 shown here is an unconditional average over the whole duration and domain of each
1372 simulation. All the vertical profiles shown here are averaged for the whole domain.

Deleted: Figure 12 shows the domain averaged vertical profiles of shortwave, longwave fluxes, and cloud fractions for the different sensitivity tests considered here. Among all the sensitivity runs, only the high-pbapPBAP case showed a noticeable effect on shortwave flux, which was 3% higher than the control run. The variations in longwave fluxes were less than 1%. The vertical profiles of cloud fraction show that a 100-fold increase in total PBAPPBAP results in a 10% higher cloud fraction between 8 and 12 km. The cloud fraction in other sensitivity runs was less sensitive to the changes in PBAPPBAP loadings.¶

1388 **6. Results from sensitivity tests about secondary ice production**

1389 Various sensitivity experiments were conducted to evaluate the role of SIP mechanisms in

1390 determining micro- and macrophysical parameters of the clouds. SIP through sublimation

1391 breakup and breakup in ice-ice collisions were switched off in the 'no-sublimation breakup'

1392 and 'no-collisional ice-ice breakup' simulations, respectively. In the 'no-secondary' case, no

1393 SIP mechanisms were active.

1394

1395 The results from these sensitivity experiments are shown in Figure 13 for the convective as

1396 well as the stratiform region of the simulated cloud. Overall, in the convective region, the no-

1397 secondary and no-collisional ice-ice breakup cases predicted 5 and 12% higher LWC

1398 respectively, than the control run (See Table 4). In the stratiform region, these cases predicted

1399 ~25% higher LWC than the control run. Lower ice number concentrations due to the absence

1400 of SIP mechanisms may reduce the rate of conversion of liquid to ice via mixed-phase

1401 processes, resulting in a higher LWC. ▼

1402

1403 In the convective part, the absence of any SIP increased ice number concentration by half an

1404 order of magnitude at temperatures warmer than -25°C. Comparing the no-SIP and control

1405 cases, the effect of the inclusion of SIP mechanisms is to increase the average ice

1406 concentration by up to half an order of magnitude at temperatures warmer than -15°C in the

1407 stratiform region. For the stratiform region, at temperatures colder than this, the absence of

1408 SIP mechanisms resulted in higher ice number concentrations by a similar magnitude. These

1409 changes at the colder levels are associated with homogeneous droplet freezing. The changes

1410 in ice number concentration in the no-collisional ice-ice breakup case are comparable with

1411 the no-secondary case. Compared to break up in ice-ice collisions, sublimation breakup has a

Deleted: ¶

<#>Fungi and bacteria¶

To investigate the role of various PBAPPBAP groups on cloud properties, model simulations were carried out by eliminating most IN active PBAPPBAP groups including FNG and BCT from the control ('no-fng' and 'no-bct' cases) run and by multiplying their initial loadings at all levels by a factor of 10 ('high-fng' and 'high-bct' cases). The resulting sensitivity experiments are then compared to the control run to understand how these PBAPPBAP groups may affect cloud properties. ¶

Deleted: The microphysical processes of AC include several SIP mechanisms such as breakup in ice-ice collisions, raindrop freezing, sublimation breakup, etc. as mentioned in Section 3.1. ...

Deleted: The SIP mechanisms, including sublimation breakup and breakup in ice-ice collisions, were turned off in the control run in the 'no-sublimation breakup' and 'no-collisional ice-ice breakup' simulations....

Deleted: 14

Deleted: In

Deleted: , the LWC (Figure 14a) between -5 to -30°C is higher than in the control run for both in the convective (~50%) and stratiform region (~80%). ...

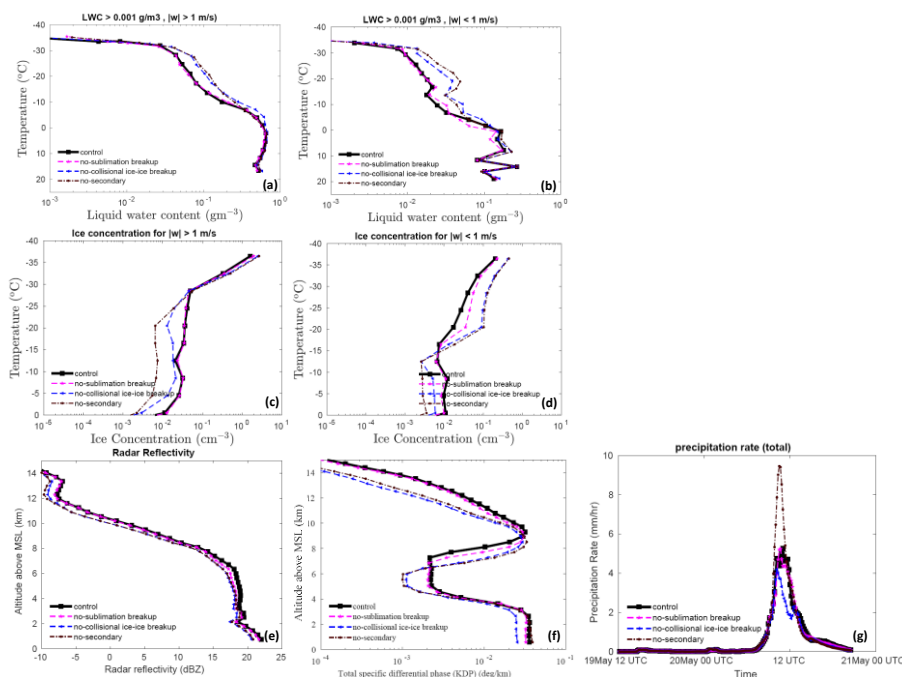
Deleted: The absence of all SIP mechanisms in the mixed-phase region results in a larger cloud droplet diameter (between 0.5 to 1 µm) (not shown here)....

Deleted: from

Deleted: A

1470 lower impact (< 40%) on the total ice number concentration in both convective and stratiform
 1471 regions.

1472



1473

1474 **Figure 13:** Temperature dependence of the liquid water content in (a) the convective and
 1475 (b) the stratiform region for ‘control’ simulation and various sensitivity runs involving SIPs.
 1476 The ice number concentration is also shown for the (c) convective and (d) stratiform regions.
 1477 The averaging conditions are mentioned at the top of each figure. The vertical profiles of (e)
 1478 radar reflectivity, (f) total specific differential phase are also shown for the same simulations.
 1479 (g) The temporal evolution of the total surface precipitation rate averaged over the domain is
 1480 also shown. All the vertical profiles shown here are averaged for the whole domain.

1481

1482

1483 The changes in simulated radar reflectivity, total specific differential phase, and surface
 1484 precipitation rate with SIP mechanisms are shown in Figures 13e, 13f, and 13g, respectively

Deleted: 14

Deleted: warmer than -25°C in the stratiform region. In the convective part, the absence of any SIP increased ice number concentration by half an order of magnitude at temperatures warmer than -15°C . At temperatures colder than this, the absence of SIP mechanisms resulted in higher ice number concentrations by a similar magnitude. The changes in ice number concentration in the no-collisional ice-ice breakup case are comparable with the no-secondary case. Compared to break up in ice-ice collisions, sublimation breakup has a lower impact (< 40%) on the total ice number concentration in both convective and stratiform regions.¶

Deleted: 14e

Deleted: 14f

Deleted: 14g

1500 for the whole storm. Overall, the simulated radar reflectivity was 1 dBZ lower in the no-SIP
1501 and no-collisional ice-ice breakup case than in the control run and can be attributed to the
1502 overall increase in ice number concentration in the control run. The no-sublimation case
1503 predicted slightly higher reflectivity than the control run. The absence of all SIPs resulted in
1504 about a 100% decrease in the K_{DP} at a temperature colder than -40°C . Between -10°C to $-$
1505 30°C , the absence of no-collisional breakup and no-secondary resulted in higher K_{DP} (half an
1506 order of magnitude) values than the control run. The absence of all SIP mechanisms results in
1507 a higher surface precipitation rate (75%) during the peak rainfall hour, which occurs around
1508 11.30 UTC compared to the control run. In the previous study, Phillips et al. (2017) have
1509 shown that SIP through ice-ice collision breakup can reduce accumulated surface
1510 precipitation in the simulated storm by 20%-40%. They attributed it to the increase in snow
1511 particles competing for available liquid and the reduction in their growth by riming. It
1512 resulted in smaller ice particles and a reduction in surface precipitation.

1513

1514

1515 7. Results about the influence of **PBAPs** in the absence of SIP mechanisms

1516 Most SIP mechanisms are highly active at temperatures above -15°C . The majority of **PBAP**
1517 showed high ice nucleation activity occurs in this part of the cloud. Most of the ice
1518 concentration in this part of the cloud is determined by various SIP mechanisms. Thus, the
1519 SIP mechanisms may influence the role of **PBAPs** in altering cloud microphysical properties.
1520 To investigate this aspect, an additional simulation was performed by eliminating all
1521 secondary ice processes from the control run and multiplying the initial loading of all **PBAP**
1522 groups by a factor of 100 (the ‘very high-**PBAP** with no SIP’ case). The results of this
1523 simulation are then compared to the no-SIP case as shown in Figure 14.

Deleted: PBAP

Deleted: PBAPs

Deleted: PBAPs

Deleted: PBAP

Deleted: pbap

Deleted: s

Deleted: 15

1531

1532 In the absence of any SIP mechanisms, the 100-fold increase in bioaerosols resulted in
1533 minimal effect on ice number concentration. Overall, without SIP the increase in bioaerosol
1534 loading by 100-fold resulted in less than a 5% change in ice number concentration. This
1535 indicates that the ice produced by various SIP mechanisms does not alter the effect of
1536 bioaerosols on-ice number concentration in the simulated clouds. The changes in simulated
1537 radar reflectivity due to a 100-fold increase in bioaerosols are negligible ($< 0.5\%$) (Figure
1538 14c). The difference in predicted surface precipitation rate and accumulated precipitation
1539 between very high-PBAP with no-secondary and no-secondary cases was lower than 3%.

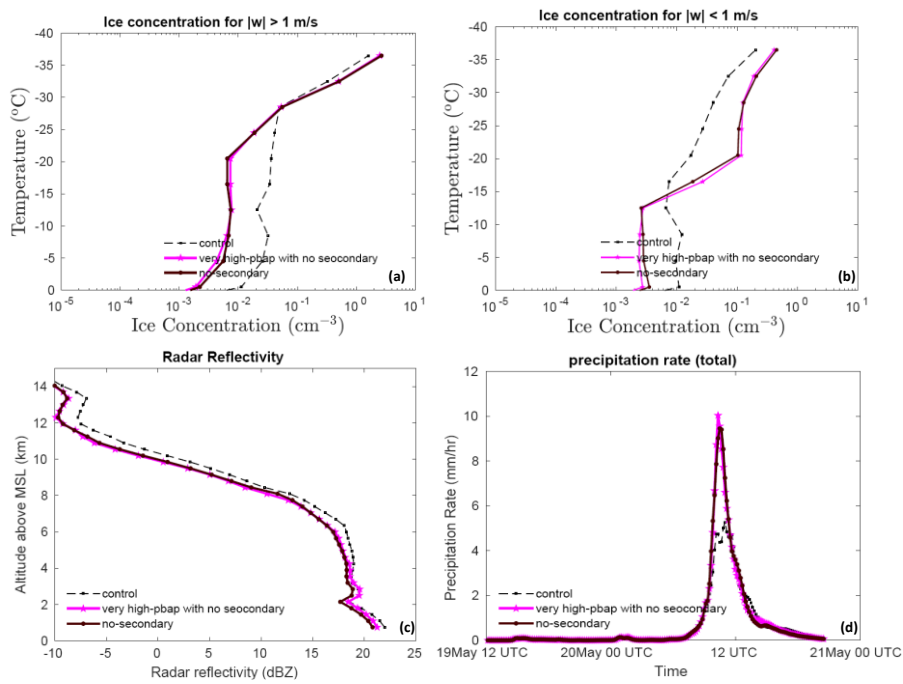
Deleted: 40

Deleted: 15c

Deleted: difference

Deleted: pbap

Deleted: 5



1540

1541 **Figure 14:** The temperature dependence of ice number concentration for the control, very
1542 high-PBAP with no SIP and no-SIP simulations averaged for (a) convective and (b)
1543 stratiform regions. The (c) vertical profile of radar reflectivity and the temporal evolution of
1544 (d) surface precipitation rate is shown for the entire simulation. All the vertical profiles

Deleted: 15

Deleted: pbap

1552 shown here are averaged for the whole domain. All the vertical profiles shown here are
1553 averaged for the whole domain.

1554

1555

1556 **8. Discussion**

1557 Five PBAP groups have been implemented in the mesoscale AC model to predict their ice
1558 nucleation activity based on the empirical formulation by PT21. The simulated concentrations
1559 of major PBAPs including fungi and bacteria are of the same order of magnitude as results
1560 from previous modeling studies (Després et al., 2012; Hoose et al., 2010b). Still, the relative
1561 abundance of PBAP groups over the simulated region is unknown due to the lack of
1562 measurements. The AC model was run with higher resolution (2 X 2 km) compared to
1563 previous studies on a global scale (Hoose et al., 2010b), to investigate the potential impact of
1564 variations in PBAP concentration on the properties of simulated squall line events more
1565 clearly.

1566

1567 Yet the control simulation is not perfectly accurate in all respects. In the stratiform region
1568 between -10 and -16°C, the predicted ice number concentration was lower than observed by
1569 aircraft by half an order of magnitude and in a fair agreement at temperatures warmer than -
1570 10°C. This uncertainty factor is similar to the uncertainty in the measurements due to various
1571 biases (e.g., Field et al. 2006. Nevertheless, all other simulated cloud microphysical
1572 parameters, radar reflectivity, and surface precipitation rate were in acceptable agreement
1573 with aircraft and ground-based observations.

1574

Deleted: ¶

Formatted: Font: Bold

Formatted: Font: Not Bold

Formatted: Font: Not Bold

Formatted: Font: Not Bold

Formatted: Font: Not Bold

Formatted: Font: Not Bold

Formatted: Font: Not Bold

Formatted: Font: Not Bold

Formatted: Font: Not Bold

Formatted: Font: Not Bold

Formatted: Font: Not Bold

1576 In the control simulation, the average ice concentration above the -30°C and -18°C levels is
1577 dominated by downwelling of homogeneously nucleated ice from above the mixed-phase
1578 region in convective and stratiform clouds respectively. Below both levels, SIP prevails. Both
1579 processes of ice initiation (homogeneous freezing and SIP) have only weak sensitivity to
1580 PBAPs, hence the weakness of the impact on simulated cloud glaciation.

Formatted: Superscript

Formatted: Superscript

1581
1582 Based on the sensitivity experiments, it can be concluded that PBAP INPs have only a limited
1583 effect on the average state of the ice phase of the simulated clouds of this mesoscale
1584 convective system. Most of the changes in ice number concentration associated with changes
1585 in PBAPs are controlled by their effects on homogeneous nucleation and SIPs. The lower
1586 dependence of simulated ice number concentration on changes in PBAPs is consistent with
1587 the findings of Hummel *et al.* (2018). Based on ensemble simulations of the regional
1588 atmospheric model for Europe, they showed that the changes in average ice crystal
1589 concentration by biological INPs are very small and are not statistically significant, implying
1590 that PBAPs play only a minor role in altering the cloud ice phase. The limited effect of
1591 PBAPs on cloud properties on a global scale has been highlighted in previous studies (Hoose
1592 et al., 2010b; Sesartic et al., 2012, 2013; Spracklen and Heald, 2014).

1593
1594 The weakness of the simulated impact from realistic PBAP fluctuations is explicable mostly
1595 in terms of the low contribution from biological ice nucleation compared to non-biological
1596 INPs to overall ice initiation. In terms of ice nucleation efficiency and onset temperatures,
1597 each PBAP group has different ice nucleation properties. Based on vertical profiles of active
1598 INPs (Figures 6), the overall contribution of activated INPs from all PBAP groups to the total
1599 active INPs was ~1%. At -15°C, temperature, the active INPs from dust and black carbon was

1600 one order higher than PBAP INPs. At -30°C, the predicted INPs from dust and black carbon
1601 were higher by one and two orders of magnitude, respectively, than PBAP INPs. The dust
1602 and black carbon INPs activated at these temperatures can be advected down to the levels
1603 where PBAP INPs are most important. Overall, this resulted in low sensitivity of the average
1604 ice phase to the changes in bioaerosol loading.

1605
1606 The ice production in the simulated cloud system at levels in the mixed-phase region (0 to -36
1607 °C) is largely controlled by various SIP mechanisms of which the most important is the
1608 breakup in ice-ice collisions. Some of these processes are active at temperatures warmer than
1609 -15°C (e.g., the HM process) where PBAP INP are important and expected to enhance the
1610 biological ice nucleation. However, our results showed that the ice production associated with
1611 SIP mechanisms is less sensitive to the initial PBAP loading because SIP causes positive
1612 feedback of ice multiplication with ice fragments growing to become precipitation-size
1613 particles that then fragment again.

1614
1615 In our study, 100-fold increase in PBAPs leads to a < 4% change in surface precipitation.
1616 Using mesoscale model simulations, Phillips et al. (2009) reported a 10% increase in
1617 accumulated surface precipitation associated with deep convective clouds due to a 100-fold
1618 increase in biological particles. Phillips et al. (2009) also noted an effect (up to 4%) on
1619 surface shortwave and TOA longwave radiation flux because of changes in PBAP number
1620 concentration. In our study, the changes in PBAP loading caused smaller changes in
1621 simulated shortwave and longwave fluxes (< 3%). Sesartic et al. (2012, 2013) showed that
1622 including fungi and bacteria in the global climate model leads to minor changes (< 0.5%) in
1623 the ice water path, total cloud cover, and total precipitation.

Formatted: Superscript

Moved (insertion) [4]

Deleted: .

Deleted: The perturbations in most active PBAPs such as fungi and bacteria showed little change in surface precipitation. ¶

1628 ▲
1629 It should be noted that the sensitivity experiments carried out in the current study are limited
1630 to the small domain (80 X 80 km domain) representing a limited area of the global
1631 ecosystem. Also, the model top was located at 16 km, and it may not represent the whole
1632 atmosphere. The results presented here are based on a mesoscale model and may not
1633 represent the global impact of PBAPs on clouds.

Formatted: Font color: Text 1

Formatted: Font color: Text 1, Not Highlight

Formatted: Font color: Text 1

Formatted: Font color: Text 1, Not Highlight

Formatted: Font color: Text 1

Formatted: Font color: Text 1, Not Highlight

Formatted: Font color: Text 1

Formatted: Font color: Text 1

1636 2. Conclusions

1637 A framework describing the ice nucleation activity of five major groups of PBAPs including
1638 fungal spores, bacteria, pollen, viral particles, plant/animal detritus, algae, and their
1639 respective fragments was provided by PT21. The ice nucleation activity of these major PBAP
1640 groups in the EP was based on samples from the real atmosphere. The present study
1641 implements this EP in AC and investigates the role of these five PBAP groups as INPs in
1642 deep convective clouds. The high-resolution (2 km horizontally) simulations over a
1643 mesoscale 3D domain (80 km wide) using AC elucidate the impact of these PBAP groups on
1644 the cloud properties. A series of sensitivity experiments were conducted to test the impact of
1645 PBAP groups on cloud properties.

Deleted: ¶

Deleted: 8

Deleted: Summary and

1646
1647 A mid-latitude squall line that occurred on 20 May 2011 during MC3E over the US Southern
1648 Great Plains is simulated with the model. The simulated number concentration of ice particles
1649 showed good agreement (to within about 50%) with aircraft observations for the convective
1650 clouds within the mesoscale system. In the stratiform region between -10 and -16°C, the

1674 model predicted ice number concentration was lower than the aircraft observation by half an
1675 order of magnitude and in a fair agreement at temperatures warmer than -10°C. Various
1676 sensitivity experiments were carried out by perturbing the initial PBAP loading and by
1677 altering various SIP mechanisms.

1678
1679 Each PBAP group has diverse properties including its shape, size, and abundance in the
1680 atmosphere. A small fraction of PBAPs is found to be ice nucleation active and can therefore
1681 act as PBAP INPs. The relative contribution of each PBAP within the total PBAPs may vary
1682 from one ecosystem to another. In the current study, their relative contribution is based on
1683 previous observations from Amazonia and can be considered as the main limitations of this
1684 study. However, the simulated number concentrations of major PBAPs including fungi, and
1685 bacteria look reasonable and are close to their typical abundance in the atmosphere.

1686
1687 Any perturbation in the PBAP concentration by factors upto 1000 assumed in the current
1688 study (resulted in maximum changes in ice number concentration by < 6% convective region
1689 and by < 40% in the stratiform region with respect to the control run. The simulations showed
1690 that simulated ice particle number concentration is much higher than the number
1691 concentrations of PBAP INPs. Even at temperatures warmer than -15°C, where PBAP INPs
1692 are thought to be the most important INP, ice crystals originated from primary heterogeneous
1693 nucleation of dust and black carbon from higher levels of the cloud frequently perturb the
1694 lower levels due to sedimentation. The major ice formation comes from SIP mechanisms and
1695 homogeneous nucleation, both are less sensitive to the changes in PBAPs. Therefore, PBAP
1696 INPs do not show a significant impact on the average ice phase of the simulated storm.▼

Deleted: ¶

Formatted: Font: (Default) Times New Roman, 12 pt

Formatted: Font: (Default) Times New Roman, 12 pt

Formatted: Font: (Default) Times New Roman, 12 pt

Formatted: Superscript

Deleted: A framework describing the ice nucleation activity of five major groups of PBAPsPBAP including fungal spores, bacteria, pollen, viral particles, plant/animal detritus, algae, and their respective fragments was provided by PT21. The ice nucleation activity of these major PBAPPBAP groups in the EP was based on samples from the real atmosphere. The present study implements this EP in AC and investigates the role of these five PBAPPBAP groups as INPs in deep convective clouds. The high-resolution (2 km horizontally) simulations over a mesoscale 3D domain (80 km wide) using AC elucidate the impact of these PBAPPBAP groups on the cloud properties. A series of sensitivity experiments were conducted to test the impact of PBAPPBAP groups on cloud properties. ¶

Formatted: Normal, Justified, No bullets or numbering

1713 PBAPs have minimal effect on the warm microphysical properties of simulated clouds. The
1714 effect on liquid water content and cloud droplet number concentration was lower than 10% in
1715 both convective and stratiform regions. Since both ice and warm microphysical processes are
1716 less sensitive to PBAPs, surface precipitation is not affected significantly by changes in
1717 PBAPs. A 100-fold increase in all PBAPs resulted in less than a 5% change in surface
1718 precipitation.

Formatted: Font: (Default) Times New Roman, 12 pt

Formatted: Normal, Left, No bullets or numbering

Formatted: Font: (Default) Times New Roman, 12 pt

Deleted: ¶

A mid-latitude squall line that occurred on 20 May 2011 during MC3E over the US Southern Great Plains is simulated with the model. The simulated number concentration of ice particles showed good agreement (to within about 10%) with aircraft observations for the convective clouds within the mesoscale system. The model predicted an ice number concentration slightly lower than the aircraft observation in the stratiform region by up to a factor of 3 between -10 and -16°C but agreed better at all other levels. This factor of 3 is similar to the uncertainty in the measurements due to various biases (e.g., Field et al. 2006), though it may also be related to the radar reflectivity there being too low (by about 8 dBZ). Nevertheless, all other simulated cloud microphysical parameters, radar reflectivity, and surface precipitation rate were in good agreement with aircraft and ground-based observations. This confirms that AC adequately reproduced the warm and cold microphysical processes of the simulated squall line case.¶

Deleted: Based on the sensitivity experiments, it can be concluded that PBAPPBAP INPs have only a limited effect on the average state of the ice phase of the simulated clouds of this mesoscale convective system. Any perturbation in the PBAPPBAP concentration resulted in changes in ice number concentration by < 5% convective region and by < 60% in the stratiform region with respect to the control run. Most of the changes in ice number concentration associated with changes in PBAPsPBAP are controlled by their effect on homogeneous nucleation. ¶

¶

The weakness of the simulated impact from realistic PBAPPBAP fluctuations is explicable mostly in terms of the low contribution from biological ice nucleation compared to non-biological INPs to overall ice initiation. In terms of ice nucleation efficiency and onset temperatures, each PBAPPBAP group has different ice nucleation properties. Based on vertical profiles of active INPs (Figures 5), the overall contribution of activated INPs from all PBAPPBAP groups to the total active INPs was ~1%. At -15°C, temperature, the predicted number of active INPs from dust and black carbon were one order higher than PBAPPBAP INPs. At -30°C, the predicted INPs from dust and black carbon were higher by one and two orders of magnitude, respectively, than PBAPPBAP INPs. Overall, this resulted in low sensitivity of the average ice phase to the changes in bioaerosol loading. ¶

Deleted: The ice production in the simulated cloud system at levels in the mixed-phase region (0 to -36 °C) is largely controlled by various SIP mechanisms of which the most important is the breakup in ice-ice collisions. In the mixed-phase region, the total ice number concentration is 1-2 orders of magnitude higher than that of active INPs. The ice production associated with SIP mechanisms is insensitive to the initial PBAPPBAP loading because SIP causes positive feedback of ice multiplication with ice fragments growing to become precipitation size particles that then fragment again. The explosive growth of ice concentrations occurs until limited by other factors. In the absence of any SIP mechanisms in the model, the effect of PBAPPBAP on the ...

1814 **Code and data availability:** Data and the code for the empirical formulation of PBAPs are
1815 available on request by contacting the corresponding author.

1816 **Competing interests:** The authors declare no conflict of interest

1817 **Author Contributions:** VJTP designed and monitored this study. SP conducted model
1818 simulation, most of the data analysis, and wrote the initial manuscript. All authors contributed
1819 to the scientific discussion and model development.

1820 **Financial support:** This work was completed for a sub-award (award number: 2019-26-03)
1821 to VTJP from a US Department of Energy (DoE) direct grant to the Ryzhkov at the
1822 University of Oklahoma (award number: DE-SC0018967). The first author was also
1823 supported by a past award from the Swedish Research Council ('VR'), which concerns
1824 modeling bio-aerosol effects on glaciated clouds (2015-05104) and Sweden's Innovation
1825 Agency (Vinnova; 2020-03406). Other co-authors were supported by a current award from
1826 the Swedish Research Council for Sustainable Development (FORMAS; award number
1827 2018-01795) and US Department of Energy Atmospheric Sciences Research Program (award
1828 number: DE-SC0018932).

1829

1830

1831

1832

1833

1834

1835

Moved up [4]: . Using mesoscale model simulations, Phillips et al. (2009) reported a 10% increase in accumulated surface precipitation associated with deep convective clouds due to a 100-fold increase in biological particles. The perturbations in most active PBAPs such as fungi and bacteria showed little change in surface precipitation.

Deleted: ¶
Our results showed that surface precipitation is not affected significantly affected by changes in PBAPsPBAP. A tenfold increase in all PBAPsPBAP resulted in less than 10% change in peak values of surface precipitation rate. Using mesoscale model simulations, Phillips et al. (2009) reported a 10% increase in accumulated surface precipitation associated with deep convective clouds due to a 100-fold increase in biological particles. The perturbations in most active PBAPs such as fungi and bacteria showed little change in surface precipitation. ¶

¶
Our results showed that the perturbations in PBAPsPBAP have only a limited effect (< 50% in number and < 15% in mass) on the ice phase as well as on precipitation. This is consistent with the findings of Hummel et al. (2018). Based on ensemble simulations of the regional atmospheric model for Europe, they showed that the average ice crystal concentration by biological INPs is not statistically significant, implying that PBAPsPBAP play only a minor role in altering the cloud ice phase. Sesartic et al. (2012, 2013) showed that including fungi and bacteria in the global climate model leads to minor changes (< 0.5%) in ice water path, total cloud cover, and total precipitation on a global scale. ¶

¶
To conclude, our simulations involving various changes in SIP indicated that peak surface precipitation rate is highly sensitive (~75%) to the inclusion of SIP mechanisms. Eliminating all SIP mechanisms from the model results in a higher and much narrower peak in surface precipitation rate. However, even in the absence of SIP mechanisms, an increase in PBAPPBAP number still causes only a minor increase in precipitation because the contribution of active PBAPPBAP INPs to the total IN activity was only 1%. ¶

¶

Deleted: PBAPs

1879 **References:**

- 1887 Blyth AM, Latham J. 1993. Development of ice and precipitation in New Mexican
1888 summertime cumulus clouds. Q. J. R. Meteorol. Soc. 119:91–120
- 1889 [Baumgardner, D., Abel, S. J., Axisa, D., Cotton, R., Crosier, J., Field, P., Gurganus, C.,
1890 Heymsfield, A., Korolev, A., Krämer, M., Lawson, P., McFarquhar, G., Ulanowski, Z.,
1891 & Um, J. \(2017\). Cloud Ice Properties: In Situ Measurement Challenges, *Meteorological
1892 Monographs*, 58, 9.1-9.23.](#)
- 1893 [Bowers RM, Lauber CL, Wiedinmyer C, Hamady M, Hallar AG, Fall R, Knight R, Fierer N.
1894 Characterization of airborne microbial communities at a high-elevation site and their
1895 potential to act as atmospheric ice nuclei. Appl Environ Microbiol. 2009
1896 Aug;75\(15\):5121-30. doi: 10.1128/AEM.00447-09](#)
- 1897 [Bauer, H., Kasper-Giebl, A., Loflund, M., Giebl, H., Hitzenberger, R., Zibuschka, F., and
1898 Puxbaum, H.: The contribution of bacteria and fungal spores to the organic carbon
1899 content of cloud water, precipitation and aerosols, *Atmos. Res.*, 64, 109–119, 2002.](#)
- 1900 [Burrows, S. M., Elbert, W., Lawrence, M. G., and Pöschl, U.: Bacteria in the global
1901 atmosphere – Part 1: Review and synthesis of literature data for different ecosystems,
1902 *Atmos. Chem. Phys.*, 9, 9263–9280](#)
- 1903
- 1904 Carlin, J. T., Reeves, H. D., & Ryzhkov, A. V. 2021: Polarimetric Observations and
1905 Simulations of Sublimating Snow: Implications for Nowcasting, *Journal of Applied
1906 Meteorology and Climatology*, 60(8), 1035-1054.
- 1907 [Chen, Q., Yin, Y., Jiang, H., Chu, Z., Xue, L., Shi, R., et al. \(2019\). The roles of mineral dust
1908 as cloud condensation nuclei and ice nuclei during the evolution of a hail storm. *Journal
1909 of Geophysical Research: Atmospheres*, 2019; 124: 14262– 14284.](#)
- 1910 Chin, M., R. B. Rood, S. J. Lin, J. F. Müller, and A. M. Thompson, 2000: Atmospheric sulfur
1911 cycle simulated in the global model GOCART: Model description and global properties.
1912 *Journal of Geophysical Research Atmospheres*, **105**, 24671–24687,
1913 <https://doi.org/10.1029/2000JD900384>.
- 1914 Crawford, I., Bower, K. N., Choularton, T. W., Dearden, C., Crosier, J., Westbrook, C.,
1915 Capes, G., Coe, H., Connolly, P. J., Dorsey, J. R., Gallagher, M. W., Williams, P.,
1916 Trembath, J., Cui, Z., and Blyth, A.: Ice formation and development in aged, wintertime
1917 cumulus over the UK: observations and modelling, *Atmos. Chem. Phys.*, 12, 4963–
1918 4985, <https://doi.org/10.5194/acp-12-4963-2012>, 2012.
- 1919 Cui, Z., and K. S. Carslaw , 2006: Enhanced vertical transport efficiency of aerosol in
1920 convective clouds due to increases in tropospheric aerosol abundance, *J. Geophys. Res.*,
1921 111, D15212, doi:10.1029/2005JD006781
- 1922 Deshmukh A., Vaughan T. J. Phillips, Aaron Bansemer, Sachin Patade, and Deepak Waman,
1923 2021: New Empirical Formulation for the Sublimational Breakup of Graupel and
1924 Dendritic Snow, DOI: <https://doi.org/10.1175/JAS-D-20-0275.1>

Després, V. R., and Coauthors, 2012: Primary biological aerosol particles in the atmosphere: A review. *Tellus, Series B: Chemical and Physical Meteorology*, **64**, <https://doi.org/10.3402/tellusb.v64i0.15598>.

DeMott P. J., A.J. Prenni, X. Liu, S.M. Kreidenweis, M.D. Petters, C.H. Twohy, *et al.* Predicting global atmospheric ice nuclei distributions and their impacts on climate Proc. Natl. Acad. Sci. U. S. A., 107 (2010), pp. 11217-11222.

DeMott, P. J. and Prenni, A. J.: New Directions: Need for defining the numbers and sources of biological aerosols acting as ice nuclei, *Atmos. Environ.*, 44, 1944–1945, 2010.

Després, V.R., Huffman, J.A., Burrows, S.M., Hoose, C., Safatov, A.S., Buryak, G., Fröhlich-Nowoisky, J., Elbert, W., Andreae, M.O., Pöschl, U., 2012. Primary biological aerosol particles in the atmosphere: a review. *Tellus B Chem. Phy. Meteorol.* 64 (1), 15598.

Dong, X., and G. G. Mace, 2003: Arctic stratus cloud properties and radiative forcing derived from ground-based data collected at Barrow, Alaska. *J. Climate*, **16**, 445–461, doi:10.1175/1520-0442(2003)016<0445:ASCPAR>2.0.CO;2.

Han, B., Fan, J., Varble, A., Morrison, H., Williams, C. R., Chen, B., et al. (2019). Cloud-resolving model intercomparison of an MC3E squall line case: Part II. Stratiform precipitation properties. *Journal of Geophysical Research: Atmospheres*, 124, 1090–1117.

Fan, J, Liu, Y-C, Xu, K-M, North, K, Collis, S, Dong, X, Zhang, GJ, Chen, Q, Kollias, P, and Ghan, SJ (2015), Improving representation of convective transport for scale-aware parameterization: 1. Convection and cloud properties simulated with spectral bin and bulk microphysics. *J. Geophys. Res. Atmos.*, 120, 3485– 3509. doi: 10.1002/2014JD022142.

Fan J., J.M. Comstock, M. Ovchinnikov, 2010: The cloud condensation nuclei and ice nuclei effects on tropical anvil characteristics and water vapor of the tropical tropopause layer *Environ. Res. Lett.*, 5 (2010), Article 044005, 10.1088/1748-9326/5/4/044005

Fan J., Bin Han, Adam Varble, Hugh Morrison, Kirk North, Pavlos Kollias, Baojun Chen, Xiquan Dong, Scott E. Giangrande, Alexander Khain, Yun Lin, Edward Mansell, Jason A. Milbrandt, Ronald Stenz, Gregory Thompson, Yuan Wang, 2017: Cloud-resolving model intercomparison of an MC3E squall line case: Part I—Convective updrafts, *J. Geophys. Res. Atmos.*, 122, 9351– 9378

Field, P. R., and A. J. Heymsfield (2015): Importance of snow to global precipitation, *Geophys. Res. Lett.*, 42, 9512–9520, doi:10.1002/2015GL065497.

Formatted: Font: Not Bold

Formatted: Line spacing: Double

Field, P. R., Heymsfield, A. J., & Bansemer, A. (2006). Shattering and Particle Interarrival Times Measured by Optical Array Probes in Ice Clouds, *Journal of Atmospheric and Oceanic Technology*, 23(10), 1357-1371.

Fridlind, A. M., and Coauthors, 2017: Derivation of aerosol profiles for MC3E convection studies and use in simulations of the 20 May squall line case. *Atmospheric Chemistry and Physics*, 17, 5947–5972, <https://doi.org/10.5194/acp-17-5947-2017>.

Fröhlich-Nowoisky, J., Kampf, C.J., Weber, B., Huffman, J.A., Pöhlker, C., Andreae, M. O., Lang-Yona, N., Burrows, S.M., Gunthe, S.S., Elbert, W., Su, H., Hoor, P., Thines, E., Hoffmann, T., Després, V.R., Pöschl, U., 2016. Bioaerosols in the Earth system: climate, health, and ecosystem interactions. *Atmos. Res.* 182, 346–376.

Garcia, E., T. C. J. Hill, A. J. Prenni, P. J. DeMott, G. D. Franc, and S. M. Kreidenweis, 2012: Biogenic ice nuclei in boundary layer air over two US high plains agricultural regions. *Journal of Geophysical Research Atmospheres*, 117, 1–12, <https://doi.org/10.1029/2012JD018343>.

Giangrande, S. E., S. Collis, A. K. Theisen, and A. Tokay, 2014: Precipitation estimation from the ARM distributed radar network during the MC3E campaign. *Journal of Applied Meteorology and Climatology*, 53, 2130–2147, <https://doi.org/10.1175/JAMC-D-13-0321.1>.

Grützun, V., O. Knöth, and M. Simmel, 2008: Simulation of the influence of aerosol particle characteristics on clouds and precipitation with LM-SPECS: Model description and first results. *Atmospheric Research*, 90, 233–242, <https://doi.org/10.1016/j.atmosres.2008.03.002>.

Hallett, J., and S. C. Mossop, 1974: Production of secondary ice particles during the riming process. *Nature*, 249, 26–28, <https://doi.org/10.1038/249026a0>.

Heymsfield, A. J., Schmitt, C., Chen, C., Bansemer, A., Gettelman, A., Field, P. R., & Liu, C. (2020). Contributions of the Liquid and Ice Phases to Global Surface Precipitation: Observations and Global Climate Modeling. *Journal of the Atmospheric Sciences*, 77(8), 2629-2648

Hoose, C., and O. Möhler, 2012: Heterogeneous ice nucleation on atmospheric aerosols: A review of results from laboratory experiments. *Atmospheric Chemistry and Physics*, 12, 9817–9854, <https://doi.org/10.5194/acp-12-9817-2012>.

Hoose, C., J. E. Kristjánsson, and S. M. Burrows, 2010: How important is biological ice nucleation in clouds on a global scale? *Environmental Research Letters*, 5, <https://doi.org/10.1088/1748-9326/5/2/024009>.

Hoose, C., Kristjánsson, J. E., Chen, J.-P., and Hazra, A.: A Classical-Theory-Based Parameterization of Heterogeneous Ice Nucleation by Mineral Dust, Soot, and Biological Particles in a Global Climate Model, *J. Atmos. Sci.*, 67, 2483–2503, <https://doi.org/10.1175/2010jas3425.1>, 2010b.

Huang S., Wei Hu, Jie Chen, Zhijun Wu, Daizhou Zhang, Pingqing Fu, Overview of biological ice nucleating particles in the atmosphere, *Environment International*, Volume 146, 2021,106197

Deleted: Forster, P., et al. (2007), Changes in atmospheric constituents and in radiative forcing, in *Climate Change 2007: The Physical Science Basis: Contribution of Working Group I to the Fourth Assessment Report of the IPCC*, edited by S. Solomon et al., pp. 131–234, Cambridge Univ. Press, New York.¶

2006 Huffman, J. A., and Coauthors, 2013: High concentrations of biological aerosol particles and
 2007 ice nuclei during and after rain. *Atmospheric Chemistry and Physics*, **13**, 6151–6164,
 2008 <https://doi.org/10.5194/acp-13-6151-2013>.

2009 Hummel, M., C. Hoose, B. Pummer, C. Schaupp, J. Fröhlich-Nowoisky, and O. Möhler,
 2010 2018: Simulating the influence of primary biological aerosol particles on clouds by
 2011 heterogeneous ice nucleation. *Atmospheric Chemistry and Physics*, **18**, 15437–15450,
 2012 <https://doi.org/10.5194/acp-18-15437-2018>.

2013 Jensen, M. P., and Coauthors, 2016: The midlatitude continental convective clouds
 2014 experiment (MC3E). *Bulletin of the American Meteorological Society*, **97**, 1667–1686,
 2015 <https://doi.org/10.1175/BAMS-D-14-00228.1>.

2016 Jaenicke, R., 2005. Abundance of cellular material and proteins in the atmospheric. *Science*
 2017 308, 73.

2018 Kanji, Z. A., Ladino, L. A., Wex, H., Boose, Y., Burkert-Kohn, M., Cziczo, D. J., & Krämer,
 2019 M. (2017). Overview of Ice Nucleating Particles, *Meteorological Monographs*, 58, 1.1-
 2020 1.33.

2021 Korolev, A. V., Kuznetsov, S. V., Makarov, Y. E., & Novikov, V. S. (1991). Evaluation of
 2022 Measurements of Particle Size and Sample Area from Optical Array Probes, *Journal of*
 2023 *Atmospheric and Oceanic Technology*, 8(4), 514-522.

2024 Korolev, A. V., Emery, E. F., Strapp, J. W., Cober, S. G., Isaac, G. A., Wasey, M., &
 2025 Marcotte, D. (2011). Small Ice Particles in Tropospheric Clouds: Fact or Artifact?
 2026 Airborne Icing Instrumentation Evaluation Experiment, *Bulletin of the American*
 2027 *Meteorological Society*, 92(8), 967-973

2028 Korolev, A., McFarquhar, G., Field, P. R., Franklin, C., Lawson, P., Wang, Z., Williams, E.,
 2029 Abel, S. J., Axisa, D., Borrmann, S., Crosier, J., Fugal, J., Krämer, M., Lohmann, U.,
 2030 Schlenczek, O., Schnaiter, M., & Wendisch, M. (2017). Mixed-Phase Clouds: Progress
 2031 and Challenges, *Meteorological Monographs*, 58, 5.1-5.50

2032 Korolev, A. and Leisner, T.: Review of experimental studies of secondary ice production,
 2033 *Atmos. Chem. Phys.*, 20, 11767–11797, <https://doi.org/10.5194/acp-20-11767-2020>,
 2034 2020.

2035 Korolev, A., Heckman, I., Wolde, M., Ackerman, A. S., Fridlind, A. M., Ladino, L. A.,
 2036 Lawson, R. P., Milbrandt, J., and Williams, E.: A new look at the environmental
 2037 conditions favorable to secondary ice production, *Atmos. Chem. Phys.*, 20, 1391–1429,
 2038 <https://doi.org/10.5194/acp-20-1391-2020>, 2020.

2039 Kumjian, M. R., and K. A. Lombardo, 2017: Insights into the evolving microphysical and
 2040 kinematic structure of northeastern U.S. winter storms from dual-polarization Doppler
 2041 radar. *Mon. Wea. Rev.*, 145, 1033–1061, <https://doi.org/10.1175/MWR-D-15-0451.1>.

2042 Knopf, D.A., Alpert, P.A., Wang, B., Aller, J.Y., 2011. Stimulation of ice nucleation by
 2043 marine diatoms. *Nat. Geosci.* 4, 88–90. <https://doi.org/10.1038/ngeo1037>

Field Code Changed

2044 Lawson, R. P., Woods, S. and Morrison, H., 2015: The microphysics of ice and precipitation
 2045 1195 development in tropical cumulus clouds, *J. Atmos. Sci.*, 72(6), 2429–2445, 1196
 2046 doi:10.1175/JAS-D-14-0274.1, 2015.

2047 Levin Z, Yankofsky S, Pardes D and Magal N. 1987. *J. Clim. Appl. Meteorol.* 26 1188–97

2048 Matus, A. V. and L'Ecuyer, T. S. (2017), The role of cloud phase in Earth's radiation budget,
 2049 *J. Geophys. Res. Atmos.*, 122, 2559– 2578, doi:10.1002/2016JD025951.

2050 Malm, W. C., J. F. Sisler, D. Huffman, R. A. Eldred, and T. A. Cahill (1994), Spatial and
 2051 seasonal trends in particle concentration and optical extinction in the United States, *J.*
 2052 *Geophys. Res.*, 99, 1347-1370.

2053 Matthias-Maser S., Berit Bogs, Ruprecht Jaenicke, The size distribution of primary biological
 2054 aerosol particles in cloud water on the mountain Kleiner Feldberg/Taunus (FRG),
 2055 *Atmospheric Research*, Volume 54, Issue 1, 2000, Pages 1-13

2056 Mattias-Maser, S., Brinkmann, J., Schneider, W., 1999. The size distribution of marine
 2057 atmospheric aerosol with regard to primary biological aerosol particles over the South
 2058 Atlantic Ocean. *Atmospheric Environment* 33, 3569–3575.

2059 Mattias-Maser, S., Jaenicke, R., 1995. The size distribution of primary biological aerosol
 2060 particles with radii > 0.2 mm in an urban/rural influenced region. *Atmospheric Research*
 2061 39, 279–286

2062 Mülmenstädt, J., Sourdeval, O., Delanoë, J., and Quaas, J. (2015), Frequency of occurrence
 2063 of rain from liquid-, mixed-, and ice-phase clouds derived from A-Train satellite
 2064 retrievals, *Geophys. Res. Lett.*, 42, 6502– 6509

2069 Möhler, O., and Coauthors, 2008: *Heterogeneous ice nucleation activity of bacteria: new*
 2070 *laboratory experiments at simulated cloud conditions.* 1425–1435 pp.
 2071 www.biogeosciences.net/5/1425/2008/.

2072 Moiseev, D. N., Lautaportti, S., Tyynela, J., and Lim, S. (2015), Dual-polarization radar
 2073 signatures in snowstorms: Role of snowflake aggregation, *J. Geophys. Res.*
 2074 *Atmos.*, 120, 12644– 12655, doi:10.1002/2015JD023884.

2075 Morris, C. E., F. Conen, J. Alex Huffman, V. Phillips, U. Pöschl, and D. C. Sands, 2014:
 2076 Bioprecipitation: A feedback cycle linking Earth history, ecosystem dynamics and land
 2077 use through biological ice nucleators in the atmosphere. *Global Change Biology*, 20,
 2078 341–351, <https://doi.org/10.1111/gcb.12447>.

2079 Murray, B. J., D. O'Sullivan, J. D. Atkinson, and M. E. Webb, 2012: Ice nucleation by
 2080 particles immersed in supercooled cloud droplets. *Chem. Soc. Rev.*, 41, 6519–6554,
 2081 <https://doi.org/10.1039/c2cs35200a>.

2082 Patade, S., Phillips, V. T. J., Amato, P., Bingemer, H. G., Burrows, S. M., DeMott, P. J.,
 2083 Goncalves, F. L. T., Knopf, D. A., Morris, C. E., Alwmark, C., Artaxo, P., Pöhlker, C.,
 2084 Schrod, J., & Weber, B. (2021). Empirical Formulation for Multiple Groups of Primary
 2085 Biological Ice Nucleating Particles from Field Observations over Amazonia, *Journal of*
 2086 *the Atmospheric Sciences*, 78(7), 2195-2220.

Deleted: ¶

2088 [Phillips, V. T. J., Donner, L. J., and Garner, S.: Nucleation processes in deep convection](#)
2089 [simulated by a cloud-system resolving model with double-moment bulk microphysics, *J.*](#)
2090 [Atmos. Sci., 64, 738–761, 2007.](#)

2091 [Phillips, V. T. J., DeMott, P. J., & Andronache, C. \(2008\). An Empirical Parameterization of](#)
2092 [Heterogeneous Ice Nucleation for Multiple Chemical Species of Aerosol, *Journal of the*](#)
2093 [Atmospheric Sciences, 65\(9\), 2757-2783.](#)

2094 Phillips, V. T. J., and Coauthors, 2009: Potential impacts from biological aerosols on
2095 ensembles of continental clouds simulated numerically. *Biogeosciences*, **6**, 987–1014,
2096 <https://doi.org/10.5194/bg-6-987-2009>.

2097 [Phillips, V. T. J., Yano, J., Formenton, M., Iltoviz, E., Kanawade, V., Kudzotsa, I., Sun, J.,](#)
2098 [Bansemer, A., Detwiler, A. G., Khain, A., & Tessendorf, S. A. \(2017\). Ice](#)
2099 [Multiplication by Breakup in Ice–Ice Collisions. Part II: Numerical Simulations, *Journal*](#)
2100 [of the Atmospheric Sciences, 74\(9\), 2789-2811.](#)

2101 [Phillips, V. T. J., Formenton, M., Kanawade, V. P., Karlsson, L. R., Patade, S., Sun, J.,](#)
2102 [Barthe, C., Pinty, J., Detwiler, A. G., Lyu, W., & Tessendorf, S. A. \(2020\). Multiple](#)
2103 [Environmental Influences on the Lightning of Cold-Based Continental Cumulonimbus](#)
2104 [Clouds. Part I: Description and Validation of Model, *Journal of the Atmospheric*](#)
2105 [Sciences, 77\(12\), 3999-4024](#)

2106 Phillips, V. T. J., J. I. Yano, and A. Khain, 2017c: Ice multiplication by breakup in ice-ice
2107 collisions. Part I: Theoretical formulation. *Journal of the Atmospheric Sciences*, **74**,
2108 1705–1719, <https://doi.org/10.1175/JAS-D-16-0224.1>.

2109 Phillips, V. T. J., P. J. Demott, C. Andronache, K. A. Pratt, K. A. Prather, R. Subramanian,
2110 and C. Twohy, 2013: Improvements to an empirical parameterization of heterogeneous
2111 ice nucleation and its comparison with observations. *Journal of the Atmospheric*
2112 *Sciences*, **70**, 378–409, <https://doi.org/10.1175/JAS-D-12-080.1>.

2113 Phillips, V. T. J., S. Patade, 2021: Multiple Environmental Influences on the Lightning of
2114 Cold-based Continental Convection. Part II: Sensitivity Tests for its Charge Structure
2115 and Land-Ocean Contrast. *Journal of the Atmospheric Sciences*,
2116 <https://doi.org/10.1175/JAS-D-20-0234.1>

2117 Phillips, V. T. J., S. Patade, J. Gutierrez, and A. Bansemer, 2018: Secondary ice production
2118 by fragmentation of freezing drops: Formulation and theory. *Journal of the Atmospheric*
2119 *Sciences*, **75**, 3031–3070, <https://doi.org/10.1175/JAS-D-17-0190.1>.

2120 Prenni, A. J., and Coauthors, 2013: The impact of rain on ice nuclei populations at a forested
2121 site in Colorado. *Geophysical Research Letters*, **40**, 227–231,
2122 <https://doi.org/10.1029/2012GL053953>.

2123 [Pörtner, Hans O., et al., 2022: Summary for policymakers. In: Climate change 2022: Impact,](#)
2124 [adaptation, and vulnerability: Summary for policy makers: Working group II](#)
2125 [Contribution to the sixth assessment report of the Intergovernmental Panel on Climate](#)
2126 [Change.](#)

Deleted: Phillips, V. T. J., and Coauthors, 2017a: Ice multiplication by breakup in ice-ice collisions. Part II: Numerical simulations. *Journal of the Atmospheric Sciences*, **74**, 2789–2811, <https://doi.org/10.1175/JAS-D-16-0223.1>.¶

Deleted: Phillips, V. T. J., and Coauthors, 2017b: Ice multiplication by breakup in ice-ice collisions. Part II: Numerical simulations. *Journal of the Atmospheric Sciences*, **74**, 2789–2811,

Deleted: Phillips, V. T. J., and Coauthors, 2020: Multiple environmental influences on the lightning of cold-based continental cumulonimbus clouds. Part I: Description and validation of model. *Journal of the Atmospheric Sciences*, **77**, 3999–4024, <https://doi.org/10.1175/JAS-D-19-0200.1>.¶

2141 Ryzhkov, A., Pinsky, M., Pokrovsky, A., & Khain, A. (2011). Polarimetric Radar
 2142 Observation Operator for a Cloud Model with Spectral Microphysics, *Journal of Applied*
 2143 *Meteorology and Climatology*, 50(4), 873-894

2144 Sahyoun, M., Wex, H., Gosewinkel, U., Šantl-Temkiv, T., Nielsen, N. W., Finster, K.,
 2145 Sørensen, J. H., Stratmann, F., and Korsholm, U. S.: On the usage of classical nucleation
 2146 theory in quantification of the impact of bacterial INP on weather and climate, *Atmos.*
 2147 *Environ.*, 139, 230–240, <https://doi.org/10.1016/j.atmosenv.2016.05.034>, 2016.

2148 Sesartic, A., U. Lohmann, and T. Storelvmo, 2012: Bacteria in the ECHAM5-HAM global
 2149 climate model. *Atmospheric Chemistry and Physics*, **12**, 8645–8661,
 2150 <https://doi.org/10.5194/acp-12-8645-2012>.

2151 Sesartic, A., U. Lohmann, and T. Storelvmo, 2013: Modelling the impact of fungal spore ice
 2152 nuclei on clouds and precipitation. *Environmental Research Letters*, **8**,
 2153 <https://doi.org/10.1088/1748-9326/8/1/014029>.

2154 Sinclair, V. A., Moisseev, D., and von Lerber, A. (2016), How dual-polarization radar
 2155 observations can be used to verify model representation of secondary ice, *J. Geophys.*
 2156 *Res. Atmos.*, 121, 10,954– 10,970, doi:10.1002/2016JD025381.

2157 Sotiropoulou, G., Ickes, L., Nenes, A. and Ekman, A.: Ice multiplication from ice–ice
 2158 collisions in the high Arctic, 2021b: sensitivity to ice habit, rimed fraction, ice type and
 2159 uncertainties in the numerical description of the process, *Atmos. Chem. Phys.*, 21, 9741–
 2160 9760, 1313 doi:10.5194/acp-21-9741-2021,

2161 Sotiropoulou, G., Vignon, E., Young, G., Morrison, H., O’Shea, S. J., Lachlan-Cope, T.,
 2162 Berne, A. and Nenes, A. 2021a: Secondary ice production in summer clouds over the
 2163 Antarctic coast: 1308 An underappreciated process in atmospheric models, *Atmos.*
 2164 *Chem. Phys.*, 21(2), 755– 1309 771, doi:10.5194/acp-21-755-2021,

2165 Spracklen, D. v., and C. L. Heald, 2014: The contribution of fungal spores and bacteria to
 2166 regional and global aerosol number and ice nucleation immersion freezing rates.
 2167 *Atmospheric Chemistry and Physics*, **14**, 9051–9059, [https://doi.org/10.5194/acp-14-](https://doi.org/10.5194/acp-14-9051-2014)
 2168 [9051-2014](https://doi.org/10.5194/acp-14-9051-2014).

2169 Szyrmer, W., Zawadzki, I., 1997. Biogenic and anthropogenic sources of ice-forming
 2170 nuclei: A review. *Bull. Am. Meteorol. Soc.* 78, 209–228.

2171 Tsushima, Y., S. Emori, T. Ogura, et al., 2006: Importance of the mixed-phase cloud
 2172 distribution in the control climate for assessing the response of clouds to carbon dioxide
 2173 increase: a multi-model study. *Clim Dyn* 27, 113–126 (2006).
 2174 <https://doi.org/10.1007/s00382-006-0127-7>.

2175 Wilson, T., and Coauthors, 2015: A marine biogenic source of atmospheric ice-nucleating
 2176 particles. *Nature*, 525, 234–238, <https://doi.org/10.1038/nature14986>.

2177 Xie, S., Y. Zhang, S. E. Giangrande, M. P. Jensen, R. McCoy, and M. Zhang, 2014:
 2178 Interactions between cumulus convection and its environment as revealed by the MC3E
 2179 sounding array. *Journal of Geophysical Research*, **119**, 11,784–11,808,
 2180 <https://doi.org/10.1002/2014JD022011>.

2181 Zhao, X., & Liu, X. (2021). Global importance of secondary ice production. *Geophysical*
2182 *Research Letters*, 48, e2021GL092581. <https://doi.org/10.1029/2021GL092581>
2183 Zuidema, P., E. R. Westwater, C. Fairall, and D. Hazen, 2005: Ship-based liquid water path
2184 estimates in marine stratocumulus. *J. Geophys. Res.*, **110**, D20206,
2185 [doi:10.1029/2005JD005833](https://doi.org/10.1029/2005JD005833).